

Utilization of dietary mixed-linkage β -glucans by the Firmicute *Blautia producta*

Received for publication, February 15, 2023, and in revised form, May 3, 2023. Published, Papers in Press, May 11, 2023.
<https://doi.org/10.1016/j.jbc.2023.104806>

Ravindra Pal Singh^{1,2,*}, Jayashree Niharika^{1,2}, Raksha Thakur², Ben A. Wagstaff³, Gulshan Kumar², Rikuya Kurata⁴, Dhaval Patel¹, Colin W. Levy³, Takatsugu Miyazaki^{4,5}, and Robert A. Field^{3,*}

From the ¹Department of Industrial Biotechnology, Gujarat Biotechnology University, Near Gujarat International Finance Tec (GIFT)-City, Gandhinagar, Gujarat, India; ²Division of Food and Nutritional Biotechnology, National Agri-Food Biotechnology Institute, SAS Nagar, Punjab, India; ³Department of Chemistry and Manchester Institute of Biotechnology, The University of Manchester, Manchester, UK; ⁴Department of Agriculture, Graduate School of Integrated Science and Technology, and ⁵Research Institute of Green Science and Technology, Shizuoka University, Shizuoka City, Shizuoka, Japan

Reviewed by members of the JBC Editorial Board. Edited by Chris Whitfield

The β -glucans are structurally varied, naturally occurring components of the cell walls, and storage materials of a variety of plant and microbial species. In the human diet, mixed-linkage glucans [MLG - β -(1,3/4)-glucans] influence the gut microbiome and the host immune system. Although consumed daily, the molecular mechanism by which human gut Gram-positive bacteria utilize MLG largely remains unknown. In this study, we used *Blautia producta* ATCC 27340 as a model organism to develop an understanding of MLG utilization. *B. producta* encodes a gene locus comprising a multi-modular cell-anchored endo-glucanase (*BpGH16_{MLG}*), an ABC transporter, and a glycoside phosphorylase (*BpGH94_{MLG}*) for utilizing MLG, as evidenced by the upregulation of expression of the enzyme- and solute binding protein (SBP)-encoding genes in this cluster when the organism is grown on MLG. We determined that recombinant *BpGH16_{MLG}* cleaved various types of β -glucan, generating oligosaccharides suitable for cellular uptake by *B. producta*. Cytoplasmic digestion of these oligosaccharides is then performed by recombinant *BpGH94_{MLG}* and β -glucosidases (*BpGH3-AR8_{MLG}* and *BpGH3-X62_{MLG}*). Using targeted deletion, we demonstrated *BpSBP_{MLG}* is essential for *B. producta* growth on barley β -glucan. Furthermore, we revealed that beneficial bacteria, such as *Roseburia faecis* JCM 17581^T, *Bifidobacterium pseudocatenuatum* JCM 1200^T, *Bifidobacterium adolescentis* JCM 1275^T, and *Bifidobacterium bifidum* JCM 1254, can also utilize oligosaccharides resulting from the action of *BpGH16_{MLG}*. Disentangling the β -glucan utilizing the capability of *B. producta* provides a rational basis on which to consider the probiotic potential of this class of organism.

The β -glucans are components of the cell walls of marine macroalgae (1), yeasts (2), staple crops (3), and bacterial exopolysaccharides (4). These complex and heterogeneous materials possess a range of backbone linkages [as in β -(1,2)-

β -(1,3)-, β -(1,3/4)- and β -(1,6)- glucans], side chain composition, and degree of polymerizations (DP) (5). Cereal β -(1,3/4)-glucans (mixed linkage glucans [MLG]) are a significant component of the cell walls of barley, oats, and rye, and are present in minor quantities in wheat (6). Cereals have been staple food for humans for millennia and are also in widespread use for livestock feed. The consumption of grain rich in soluble MLG correlates with benefits for the cardiovascular system, giving rise to reduced risk of coronary heart disease (7). While efforts to determine the metabolism of MLG in Gram-negative bacteria (e.g., *Bacteroides ovatus*) have been reported (8), the corresponding processes in Gram-positive bacteria remain to be established, as do the full details of routes to beneficial health impact.

The human genome encodes a modest repertoire of Carbohydrate-Active enZymes (CAZymes) (9), including those associated with the cleavage of α -linked glucans, such as starch (10). However, the MLGs are not recognized by human genome-encoded digestive enzymes, resulting in their passage through the digestive system to the lower gastrointestinal tract (GIT). These dietary MLGs become food for the human gut microbiota (HGM), influencing the composition of the microbial community and the metabolites that they produce (11). The HGM predominantly consists of bacteria belonging to *Bacteroidetes*, *Actinobacteria*, *Proteobacteria*, and *Firmicutes* (12). It is estimated that bacterial communities of these phyla collectively harbor ~150-fold more genes than the host genome and that they have an underlying impact on host physiology (13). These bacterial genes comprise a variety of CAZymes and transporters, which play a crucial role in facilitating host metabolism through the digestion of complex glycans (14, 15). Among the downstream metabolites arising from dietary polysaccharide degradation, butyrate primarily provides energy to colonocytes (16), supporting an anti-carcinogenic, anti-inflammatory environment, and strengthening gut barrier functions (16, 17). In contrast, acetate primarily nourishes gut-beneficial bacteria (18), helping to maintain gut microbial homeostasis. It also crosses the blood-brain barrier and is a source of energy for the brain (19).

* For correspondence: Ravindra Pal Singh, ravindra.singh@gbu.edu.in; Robert A. Field, robert.field@manchester.ac.uk.

Utilizing mixed-linkage β -glucans by the *Blautia producta*

Short- or long-term therapeutic intervention, for instance with antibiotics, can impact the gut microbiome, leading to dysbiosis and altering functional and metabolic activities (20). Improving understanding in this space, accompanied by a better molecular understanding of the mechanisms by which individual members of the microbiota utilize complex glycan, is expected to contribute substantially to the rational development of nutritional or therapeutic interventions that restore gut homeostasis and normal gut function.

The utilization of complex glycans by members of Gram-negative *Bacteroidetes* is well known, with associated organisms possessing gene clusters, so-called Polysaccharide Utilization Loci (PULs) (21, 22). A representative structure for barley MLG is shown in Figure 1A; other glucans with a β -1,3-linked backbone include curdlan (unbranched) (4), laminarin (β -1,6 linked single glucose as side chains) (1, 23), and yeast β -glucan (long β -1,6-linked glucan side chains)- such β -1,6-

linked glucan side chains absent in cereals (8, 24, 25). An MLG-utilizing molecular mechanism has been identified in the Gram-negative bacterium *B. ovatus* ATCC 8483 (8), where a gene locus centered on tandem *susC/susD* homologs that code for the TonB-dependent transporter (TBDDT or *SusC*), extracellular anchored endo-acting enzyme (*BoGH16_{MLG}*), periplasmic exo-acting enzyme (*BoGH3_{MLG}*) and the cell-surface glycan-binding protein (*BoSGBP-A* and *BoSGBP-B*) (Fig. 1B). *BoSGBP-B* attaches to MLGs in the gut lumen and *BoGH16_{MLG}* cleaves them into oligosaccharides, which are trapped by the *SusD* homolog (*BoSGBP-A*) of a transporter and are brought into periplasmic space by a *SusC* transporter. Once they are inside the cell, *BoGH3_{MLG}* cleaves these oligosaccharides into glucose, which is subsequently transported into the cytoplasm for further metabolism. In contrast, although Gram-positive *Firmicutes* phylum is dominant in the HGM, little is known about how members of this phylum

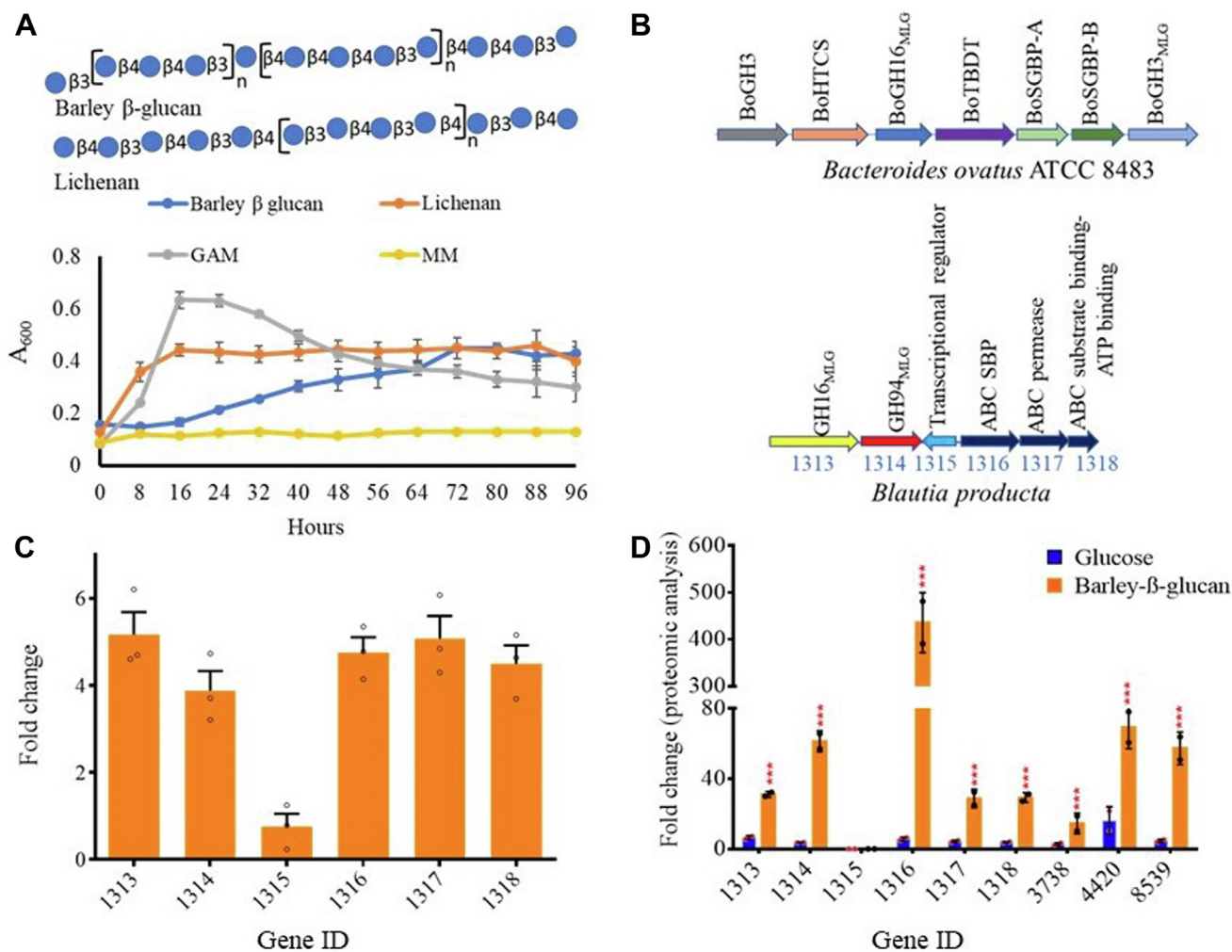


Figure 1. Growth and regulation of a β -glucans utilization locus in *Blautia producta*. A, representative structures of barley β -glucan and lichenan as per symbolic nomenclature for glycans (<https://www.ncbi.nlm.nih.gov/glycans/snfg.html>). Growth of *B. producta* was performed on a minimal medium (MM) containing 1% barley β -glucan or lichenan. B, β -glucan utilization locus in *B. producta* and the corresponding locus of *Bacteroides ovatus* ATCC 8483 (8). C, gene expression analysis of β -glucan utilization locus through RT-qPCR after growing cells of the *B. producta* on a MM containing 1% barley β -glucan. Changes in the expression level of these genes present in the locus were calculated as fold change and RT-qPCR data were normalized to 16S rRNA transcript levels. D, in addition to genes present in the locus, other cytoplasmic genes involved in the utilization of barley β -glucan were identified through proteomics. Proteomic data represent two replicates, and differences in expression levels between glucose and barley β -glucan growth cultures were analyzed by two-way ANOVA ($***p = 0.001$). GAM, Gifu anaerobic medium. UniProt IDs for *bp3738*, *bp4420*, and *bp8539* are A0A6P1Z_{5U5}, A0A6P1Z_{AR8}, and A0A6P1Y_{X62} respectively.

utilize MLG. *Firmicutes* typically lack the repertoire and organization of genes present in *Bacteroides* PULs (26) and display different approaches for utilizing dietary glycans, as identified in *Roseburia* for mannan (27). In particular, Sheridan *et al.* (26) identified that Gram-positive PUL (gpPULs) of *Roseburia* and *Eubacterium rectale* typically consist of glycoside hydrolases, ABC transport proteins, and transcriptional regulator genes.

Firmicute *Blautia producta* ATCC 27340 is an anaerobic cocci-shaped bacterium of the Lachnospiraceae family. It is commonly present in the human GIT, and it has recently been reported as a potential probiotic (28) by virtue of its ability to eliminate inflammatory and metabolic diseases (28) and restore colonization resistance against vancomycin-resistant *Enterococcus* (29, 30). While established as an important species in the GIT, the mechanistic basis of its nutritional impact remains elusive. Our previous study (31) showed that *B. producta* can grow on β -(1,3)-linked short-length glucans, but the mechanism by which it processes such glucans to glucose for further metabolism remains unknown. Here we use an interdisciplinary approach to unravel the molecular mechanism employed by *B. producta* to depolymerize MLG. Our findings show that the growth of *B. producta* on MLG is highly dependent on the expression of a gene locus encoding a multi-modular cell-anchored endo-glucanase, an ABC transporter, intracellular β -glucosidase, and intracellular phosphorylases. These proteins work in concert to effect complete degradation of MLG to glucose or/and glucose-1-phosphate. Through whole-cell experiments, we demonstrate that *B. producta* endo-glucanase can facilitate cross-feeding on MLG-derived β -glucans to various beneficial bacterial species. Overall, this study confirms the potential for developing targeted intervention strategies to improve human health by manipulating the gut microbiota with dietary mixed-linkage β -glucans.

Results

Growth of *B. producta* and identification of a β -glucan utilization locus

B. producta ATCC 27340 was able to grow on barley and lichenan MLG as well as Gifu anaerobic medium (GAM - used as a control) (Fig. 1A), and genes that may allow this to happen were identified using the JGI/IMG online server (32). An open reading frame encoding the β -(1,3/4)-glucanase of *B. ovatus* ATCC 8483 (*BoGH16_{MLG}*) (8) was chosen as a query sequence for BlastP analysis of the genome of *B. producta* (33). This led to the identification of a putative *B. producta* β -(1,3/4)-glucanase, with a predicted 33% amino acid similarity in its catalytic domain to the *B. ovatus* sequence. Distinct from its *B. ovatus* (~30 kDa) counterpart, *BpGH16_{MLG}* contains four CBM4 family carbohydrate-binding modules (<http://www.cazy.org/>), leading to a larger molecular weight of ~130 kDa. Genomic analysis with this lead *B. producta* sequence identified a locus comprising genes for a putative endo β -glucanase (*bp1313*-*BpGH16_{MLG}*), cellobiose phosphorylase (*bp1314*), an

AraC-type DNA-binding protein (*bp1315*), and genes for an ATP binding cassette (ABC) transporter (substrate-binding protein- SBP, permease protein and ABC subunits couple the binding/hydrolysis of ATP, *bp1316*-*bp1318*) (Fig. 1B).

To confirm the involvement of this gene locus in the utilization of MLG, *B. producta* was cultured on barley β -glucan, and RT-qPCR was employed to evaluate the transcriptional level of the locus-associated genes. The genes encoding *bp1313* and *bp1314* were upregulated by 5.2 and 3.9-fold, respectively, in the presence of barley β -glucan compared to growth on glucose. Phylogenetic analysis of Bp1313 and Bp1314 established them as a β -glucanase (GH16 family) and a glucan phosphorylase (GH94 family), hereafter referred to as *BpGH16_{MLG}* and *BpGH94_{MLG}* (Figs. S1 and S2). Expression of *bp1316*, *bp1317*, and *bp1318* was upregulated by 4.7-, 5-, and 4.5-fold for growth on barley MLG *versus* glucose, respectively (Fig. 1C). A 0.76-fold upregulation of transcriptional regulator *bp1315* was observed for growth on barley β -glucan compared to glucose; a similarly modest change in expression of a transcriptional regulator was previously observed for the utilization of mannan (27). We next compared the proteomes of *B. producta* grown on barley β -glucan *versus* glucose: among CAZymes, five proteins were abundant (Fig. 1D). Bp1313 and Bp1314 were expressed in abundance by approximately 5- and 16-fold on barley β -glucan compared to glucose. Proteomic analyses did not detect membrane-bound Bp1315 under either set of growth conditions. The production of *BpSBP* (Bp1316) increased by 77-fold, whereas Bp1317 and Bp1318 were expressed by about 7-fold each. Among these proteins, one protein (Bp3738) belongs to CAZy family GH18, and two proteins (Bp4420 and Bp8539) belong to GH3; they were upregulated by 5.1, 3.4, and 12.4-fold, respectively. An NCBI Conserved Domain database search highlighted that Bp3738 may not act on β -glucan (34). Furthermore, this analysis suggested that Bp3738 may cleave chitin, as similar domain-containing enzymes have previously been characterized (<http://www.cazy.org/GH18.html>). Thus, further analysis was not performed on this protein.

Cellular localization and enzymatic activity of *BpGH16_{MLG}*

Cellular localization

BpGH16_{MLG} is implicated in the cell surface cleavage of MLG in *B. producta*, an essential first step for barley β -glucan utilization. Accordingly, LipoP 1.0 predicted a type I signal sequence (score = 14.00) in its N-terminal region (35). To confirm the prediction of cell surface association, *B. producta* cells grown in a minimal medium containing 1% barley β -glucan were subjected to immunolocalization studies with custom polyclonal antisera raised against rec*BpGH16_{MLG}*. The *BpGH16_{MLG}* was clearly visualized on the outer surface of bacterial cells (Fig. 2A). Similar experiments using custom antisera raised against rec*BpGH94_{MLG}* gave no fluorescent signal (Fig. 2B), consistent with the expected intracellular expression of *BpGH94_{MLG}*. Indeed, no signal peptide was predicted for this protein when analyzed with SignalP, v. 4.0

Utilizing mixed-linkage β -glucans by the *Blautia producta*

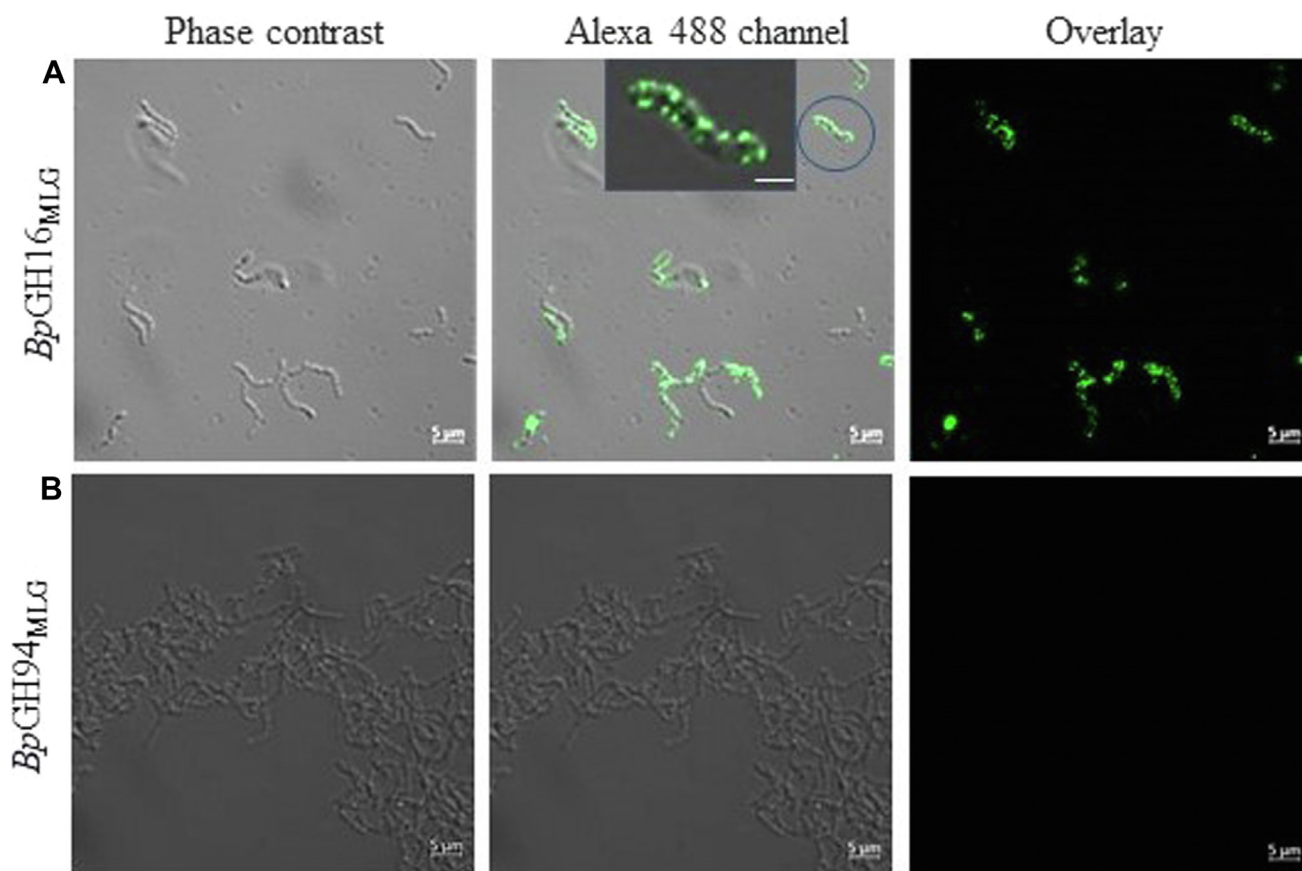


Figure 2. Enzyme localization analysis. A and B, phase-contrast confocal microscopy, corresponding fluorescence microscopy, and merged images of *B. producta* cells grown on a minimal medium containing barley β -glucan as the sole carbon source. Cells were probed with custom polyclonal antibodies against recBpGH16_{MLG} (A) and recBpGH94_{MLG} (B). Insert shows zoomed-in view of the bacterial surface revealing that BpGH16_{MLG} is present at the outer membrane of a cell. Scale bar for zoom image and all other images are 0.5 μ m and 5 μ m, respectively.

(36). Despite this, it has the potential for binding with BpGH94_{MLG} as shown in Fig. S3.

Enzymatic activity of BpGH16_{MLG}

The optimum temperature and pH for recombinant BpGH16_{MLG} were determined to be 37 °C and pH 5.7 (phosphate buffer), respectively (Fig. S4). In the initial screening, BpGH16_{MLG} did not show activity with maltose [α -(1,4)-linked glucose], gentiobiose [β -(1,6)-linked glucose], cellobiose [β -(1,4)-linked glucose], celotriose [β -(1,4)-linked glucose], laminaribiose [β -(1,3)-linked glucose], and sucrose [α -(1,2)-linked glucose and fructose] (Fig. S5A). It did cleave oat β -glucan, yeast β -glucan, lichenan, lentinan, laminaritriose, laminarin, and barley- β -glucan (Fig. S5, B–E), suggesting that it has a cleavage specificity for β -(1,3)-linked glucans and a minimum trisaccharide is required for its activity. Subsequent Michaelis-Menten kinetic analysis revealed a higher specificity constant (k_{cat}/K_m) for barley β -glucan and lichenan over laminarin and oat β -glucan, respectively (Table 1 and Fig. S6). Kinetic parameters and potent activity of BpGH16_{MLG} on barley β -glucan and lichenan as compared to laminarin (Table 1 and Fig. S7, A–E) suggest that this enzyme is β -(1,3/4) glucanase with an ability to cleave β -(1,3)-linked glucans (37). Although

BpGH16_{MLG} is highly active on laminarin, it does not support the growth of *B. producta* on this (31), which may indicate that the structural features of laminarin are unable to activate the gpPUL.

Generation of a limit digest for barley β -glucan with BpGH16_{MLG} yielded tri- and tetra-saccharide products (Fig. 3A), as evidenced by TLC and MALDI-TOF-MS analyses (Fig. S7, C and D). Using a combination of fluorophore-assisted carbohydrate electrophoresis (FACE) (Fig. S8A), MALDI-TOF-MS (Fig. S8, B and C) and NMR analysis (Fig. S8D), these glucans were confirmed to be Glc- β -(1,4)-Glc- β -(1,4)-Glc- β -(1,3)-Glc- [hereafter G4G4G3G] and Glc- β -(1,4)-Glc- β -(1,3)-Glc- [hereafter G4G3G]. The same glucans were previously identified as the limit cleavage from the action of *B. ovatus* BoGH16_{MLG} (8), which is to be expected based on the sequence similarity of the catalytic domains of the two enzymes. Further analysis suggested that the catalytic domain of BpGH16_{MLG} belongs to subfamily GH16_3 (38), along with BoGH16 (Fig. S1).

Structure modeling of BpGH16_{MLG} was performed using AlphaFold2 (Fig. 3B) and predicted local distance difference test (pLDDT- Figs. 3C and S9) (39, 40). The model structure of BpGH16_{MLG} (green) was superimposed on BoGH16_{MLG} (cyan) in complex with G4G4G3G (PDB 5NBP, magenta stick) in order to identify essential catalytic

Table 1
Kinetic parameters of native and mutant *Bp*GH16 on various β glucans

Enzyme	Substrate	K_m (mg ml ⁻¹)	k_{cat} (s ⁻¹)	k_{cat}/K_m (s ⁻¹ mg ⁻¹ ml)
<i>Bp</i> GH16	Laminarin	0.24 ± 0.03	43 ± 0.6	179
	Lichenan	0.13 ± 0.02	36 ± 0.5	275
	Barley β -glucan	0.22 ± 0.04	62 ± 1.2	281
	Oat β -glucan	0.32 ± 0.05	46 ± 0.8	148
Mutant	Substrate	K_m (mg ml ⁻¹)	k_{cat} (s ⁻¹)	k_{cat}/K_m (s ⁻¹ mg ⁻¹ ml)
R331A	Barley- β -glucan	0.35 ± 0.05	48 ± 0.8	137
L358A		0	0	0
E379A		0	0	0
D381A		0.17 ± 0.04	35.7 ± 1.1	210
E384A		0	0	0
W362A		0	0	0
H398A		0	0	0

Maltose was used to generate a standard curve. Kinetic parameters of mutant enzymes were determined with barley β -glucan in order to demonstrate the role of each residue in overall activity. Kinetic parameters were performed using DNS assay McKee (84).

residues and to provide insight into *Bp*GH16_{MLG} substrate binding (Fig. 3D). A signature sequence, EXDXXE, is generally present in the active site of mixed-linkage endo- β -glucanases belonging to GH16 (41). This signature sequence is also present in the active site of the *Bp*GH16_{MLG}, where the first and last 'E' and D represent E379, E384, and D381, respectively (Fig. 3E). Alanine scanning mutagenesis on these and other residues present at the putative active site was performed, based on structural alignment (Fig. 3E). As

expected, mutation of the catalytic nucleophile (E379A) or the catalytic base (E384A) of the EXDXXE motif gave rise to inactive enzymes. In contrast, mutation of the electrostatic helper (D381A) resulted in a 1.7-fold reduction in k_{cat} , accounting for an overall 1.34-fold loss in activity on barley β -glucan (Table 1). For other active site residues (Fig. 3E): R331A had a modest impact on K_m (<2-fold increase) and k_{cat} (~1.3-fold reduction); L358A, W362A, and H398A led to inactivation of the enzyme.

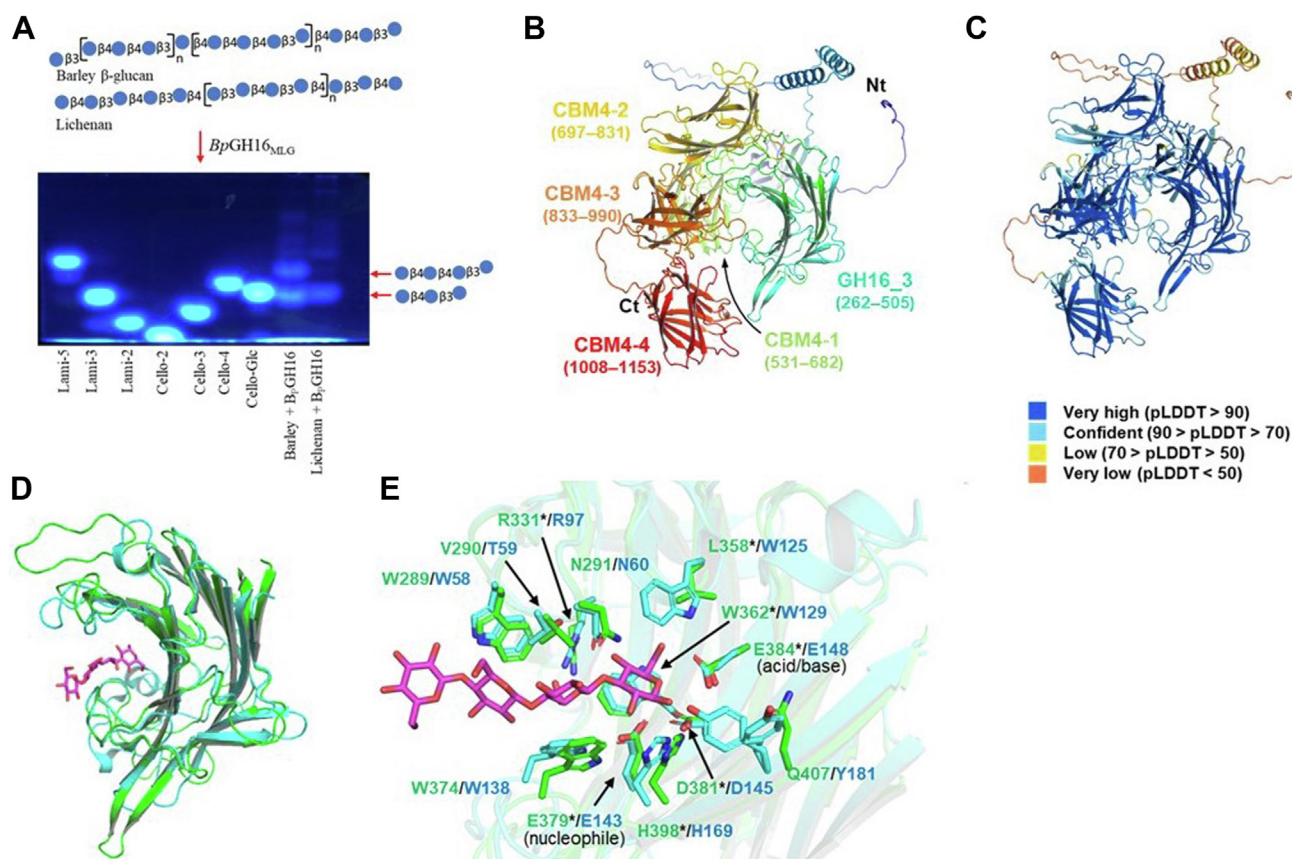


Figure 3. AlphaFold2 structure prediction and identification of critical residues of *Bp*GH16_{MLG} from *B. producta* ATCC 27340. A, oligosaccharides obtained from the *Bp*GH16_{MLG} hydrolyzed barley- β -glucan and lichenan were fluorescently tagged and run onto a 37% polyacrylamide gel electrophoresis. B, the AlphaFold2 model of full-length *Bp*GH16_{MLG}. The ribbon model is colored in a rainbow from N terminus (Nt, blue) to C terminus (Ct, red). The GH16 subfamily three catalytic domains (GH16_3) and four CBM4 domains (CBM4-1 to CBM4-4) are indicated with residue numbers in parenthesis. C, the ribbon model is colored based on pLDDT score. D, superimposition of *Bp*GH16_{MLG} (green) on *Bo*GH16_{MLG} (cyan) in complex with G4G4G3G (PDB 5NBP, magenta stick). E, comparison of active sites of *Bp*GH16_{MLG} (green) and *Bo*GH16_{MLG} (cyan). The residues mutated to alanine in this study are labeled with asterisk. G4G4G3G is shown in magenta.

Utilizing mixed-linkage β -glucans by the *Blautia producta*

As noted above, *BpGH16_{MLG}* contains four CBM4 family carbohydrate-binding modules following the GH16 catalytic domain (residues 262–505): CBM4_1 (531–682), CBM4_2 (697–831), CBM4_3 (833–990), and CBM4_4 (1008–1153) (Fig. 3B) as predicted with DeepTMHMM (42). A similar arrangement of four homologous CBMs was previously reported in the lichenase A/laminarinase (LicA) from *Clostridium thermocellus* (*CtCDP*) (43). The *BpGH16_{MLG}* CBMs show little to no sequence similarity to each other: while *BpCBM4_1* showed 25% sequence similarity to *BpCBM4_4*, *BpCBM4_2*, and *BpCBM4_3* do not show any sequence similarity with other *B. producta* CBM4s. However, *BpCBM4_1*, *BpCBM4_2*, *BpCBM4_3*, and *BpCBM4_4* revealed 33%, 28%, 40%, and 41% sequence similarity with *CtCBM4_1*, *CtCBM4_2*, *CtCBM4_3* and *CtCBM4_4*, respectively. Interestingly, the kinetic parameters for *BpGH16_{MLG}* and *BoGH16_{MLG}* with barley MLG are rather similar, with K_m 0.22 ± 0.04 and 0.364 ± 0.051 , and k_{cat} 62 ± 1.23 and 85.8 ± 4.6 , respectively, suggesting that the CBMs afford no direct kinetic advantage to the *Blautia* enzyme. Although the CBMs appear not to matter for the hydrolysis of MLG in dilute solution under the assay conditions, they might play an important role in binding to insoluble plant cell wall digestion in the complex environment of the GIT.

Recognition and uptake of oligosaccharides released by *BpGH16_{MLG}*

Next, we focused on the solute binding protein (SBP) of the ABC transporter which was expected to have a carbohydrate-binding role. Gram-positive bacteria use SBPs to capture oligosaccharides from the extracellular environment for carbon utilization (44–46). Oligosaccharides captured by SBPs are released into the periplasm of the ABC transporter, which is formed of two transmembrane domains where the translocation of oligosaccharides is coupled with ATP hydrolysis by the cytoplasmic nucleotide-binding domain (47). Although functions of SBPs for utilization of some oligosaccharides in other members of the Lachnospiraceae are known (e.g., *Roseburia*) (27), utilization of β -glucans has not been studied to date.

The LipoP-1.0 and SignalP, v. 4.0 servers suggested that *BpSBP_{MLG}* has an N-terminal lipid-anchored signal peptide sequence (score = 17.4). Consequently, *BpSBP_{MLG}* without signal sequence was cloned into a pET28a(+) and the protein

was expressed in *Escherichia coli*, giving high levels of recombinant protein (~ 80 mg/L). The thermodynamic parameters for binding of various oligosaccharides by *BpSBP_{MLG}* were evaluated by ITC (Table 2 and Fig. S10). *BpSBP_{MLG}* showed no detectable affinity for maltose, gentiobiose or lactose, but displayed some affinity towards cellobiose and laminaribiose, while the corresponding trisaccharides and mixed linkage G4G3G were bound 9 to 30 times more tightly (Table 2 and Fig. S10). Additionally, the *BpSBP_{MLG}* could also accommodate cellotetraose ($K_d = 0.75 \mu\text{M}$), G4G4G3G ($K_d = 5.14 \mu\text{M}$), and laminaritetraose ($K_d = 5.6 \text{ mM}$), indicating a preference for β -(1,4)-linked-oligosaccharides. In terms of binding stoichiometry (n), G4G4G3G showed $n = 0.77$ when compared to 0.45 for cellotetraose, suggesting a preference for linear tetrasaccharide binding (Table 2). The β -mannooligosaccharide binding protein of *Roseburia* displayed similar binding affinity to mannotetraose with K_d and n values of $3.89 \mu\text{M}$ and 0.7, respectively (27).

In order to better understand the importance of the *BpSBP_{MLG}* in the utilization of β -linked oligosaccharides, a targeted gene deletion strategy was first time employed for *B. producta*. Adapting the strategy previously developed for *Bifidobacterium longum* (48) (Fig. S11), we used a double-crossover markerless system for the deletion of the *BpSBP_{MLG}*-encoding *bp1316* gene in the *B. producta* genome. Following confirmation of gene deletion, we observed that *B. producta* Δ SBP showed significant retardation in growth on a minimal medium containing 1% barley β -glucan as compared to the wild-type strain (Fig. 4A). The data confirm the central role of *BpSBP_{MLG}* in enabling *B. producta* growth on MLG.

Various attempts to crystallize the recombinant *BpSBP_{MLG}* were performed in order to determine the molecular basis for the oligosaccharide binding as mentioned in the Supplementary file. However, no crystals were obtained, even after truncation of the flexible N-terminal region of the protein. Instead, AlphaFold2 was employed to predict the three-dimensional structure of *BpSBP_{MLG}* (31, 39, 40). The generated model adopted a typical SBP fold that consists of two α/β folds (Fig. 4B) and was similar to the structures of known sugar-binding proteins classified into cluster D class I (D-I subcluster) (49). The three-dimensional structures of some β -glucoside-binding proteins have been reported (50–52), and they are classified into the C-II or D-I subclusters. The CD

Table 2
Thermodynamics of binding of oligosaccharides to *SBP_{MLG}* measured by ITC at 25 °C in 10 mM in sodium phosphate (pH 7.0)

Ligand	Representative images	K_d (M)	ΔG^0 (kcal mol ⁻¹)	ΔH (kcal mol ⁻¹)	$-\Delta S^0$ (kcal mol ⁻¹)	n
G4G3G		$(1.01 \pm 0.1) \times 10^{-6}$	-8.18	-12.6 ± 0.32	4.4	0.42 ± 0.01
G4G4G3G		$(5.14 \pm 0.01) \times 10^{-6}$	-7.22	-12.9 ± 0.85	5.7	0.77 ± 0.02
Cellobiose		$(30.6 \pm 7.09) \times 10^{-6}$	-6.2	-7.0 ± 2.2	0.8	0.78 ± 0.18
Celotriose		$(1.74 \pm 0.33) \times 10^{-6}$	-7.9	-7.1 ± 0.31	0.8	0.77 ± 0.02
Cellotetraose		$(0.75 \pm 0.03) \times 10^{-6}$	-8.35	-16.6 ± 0.75	8.25	0.45 ± 0.02
Laminaribiose		$(22.1 \pm 0.93) \times 10^{-6}$	-6.35	-3.14 ± 0.16	2.94	1.03 ± 0.02
Laminaritriose		$(3.41 \pm 0.01) \times 10^{-6}$	-7.46	-3.66 ± 0.02	3.8	0.9 ± 0.01
Laminaritetraose		$(5.6 \pm 2.12) \times 10^{-3}$	-5.43	-0.15 ± 0.12	5.29	ND

G4G3G: Glc- β -1-4-Glc- β -1-3-Glc, and G4G4G3G: Glc- β -1-4-Glc- β -1-4-Glc- β -1-3-Glc. ND-not determined. The *BpSBP_{MLG}* did not bind with maltose, gentiobiose and lactose.

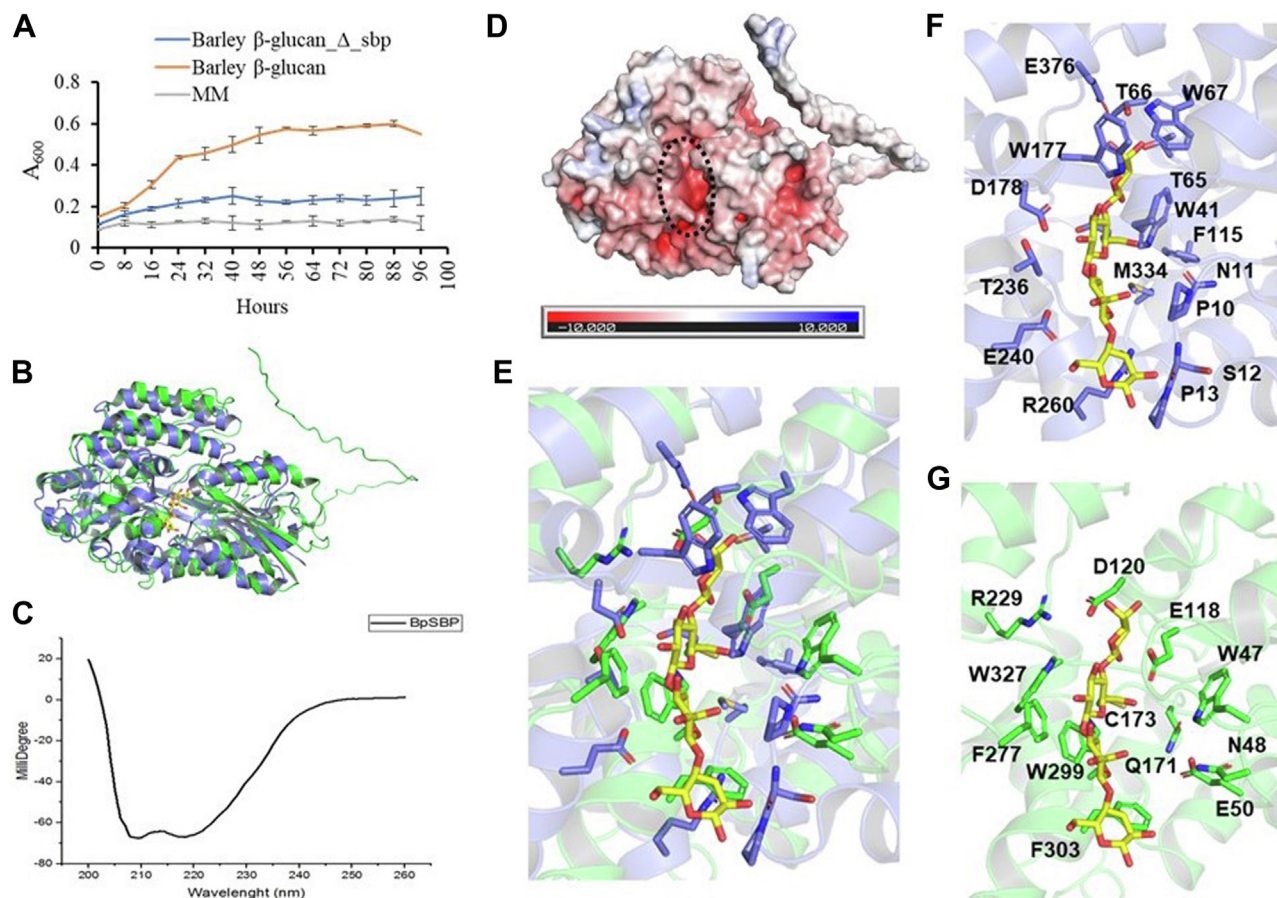


Figure 4. Growth of mutant *B. producta* Δ sbp on barley β -glucan and structure prediction of *BpSBP*_{MLG}. *A*, the growth curve of *B. producta* and mutant *B. producta* Δ sbp on a minimal medium containing 1% barley β -glucan. *B*, structural comparison of the *BpSBP*_{MLG} model (green) and the crystal structure of *Thermus thermophilus* β -glucoside-binding protein β GlyBP (sequence similarity, 20%) in complex with celotetraose (PDB 7C68, slate blue). Celotetraose is shown as a yellow stick model. *C*, circular dichroism spectrometry of *BpSBP*_{MLG}. *D*, electrostatic potential of surface model of *BpSBP*_{MLG} generated by AlphaFold2. The putative sugar-binding site of *BpSBP* is indicated as a dotted ellipse. *E*, overlay structure sugar-binding sites of β GlyBP and *BpSBP*_{MLG}. *F–G*, the sugar-binding sites of β GlyBP (*F*) and *BpSBP*_{MLG} (*G*) and their superposition (*E*). celotetraose (thin yellow stick) of PDB 7C68 is superimposed to *BpSBP*_{MLG}.

spectrum also supported that this protein contains predominantly α -helices (Fig. 4C). The β -glucoside-binding protein (β -GlyBP) of *Thermus thermophilus* belongs to the D-I subcluster and binds β -(1,2), β -(1,3), β -(1,4) and β -(1,6)-linked glucooligosaccharides (52). Based on the surface electrostatic potential, the cleft between two α/β domains is negatively charged and is predicted to be the ligand-binding site (Fig. 4D). Although *BpSBP*_{MLG} has only 20% sequence similarity to β GlyBP, the overall structures and positions of the sugar-binding sites are similar (Fig. 4, B and D). The amino acid residues that bind the ligands in β GlyBP were not conserved in *BpSBP*_{MLG}, but several aromatic residues were found in the putative binding site of *BpSBP*_{MLG} (Fig. 4, E and G). The amino acid residues in the predicted sugar-binding site are highly conserved between *BpSBP*_{MLG} and its relatively close orthologues (Fig. S12).

Cytoplasmic digestion of mixed-linkage oligosaccharides by phosphorylases

Next, we focused on the cytoplasmic degradation of oligosaccharides trapped and imported by the *BpSBP*_{MLG} and its associated ABC transporter. Locus-associated gene *bp1314*

was predicted to encode a cellodextrin phosphorylase (CDP) belonging to CAZy family GH94. The recombinant *BpGH94*_{MLG} showed maximum activity between pH 6.5 to 7.4 in HEPES buffer at 37 °C using 10 mM inorganic phosphate and celotriose (Fig. S13). The *BpGH94*_{MLG} did not show any phosphorolysis activity against laminaribiose, laminaritriose, cellobiose, gentiobiose, maltose, and sucrose (Fig. S14, A–C). The *BpGH94*_{MLG} cleaved celotriose and G4G3G, suggesting that it is a β -(1,4)-glucose phosphorylase (Fig. S14, A and B). It catalyzed phosphorolysis of barley β -glucan and mainly produced laminaribiose, cellobiose, and glucose-1-phosphate (Glc-1-P) (Fig. S14, D–E).

Kinetic parameters for phosphorolysis of celotriose, G4G3G, and G4G4G3G showed that K_m was about 1.85-fold lower and 0.75-fold higher for G4G3G and G4G4G3G, respectively, when compared to celotriose (Fig. S15 and Table 3). Higher k_{cat}/K_m was observed for G4G4G3G by 2.4 and 1.6-fold when compared to celotriose and G4G3G, respectively. Similarly, k_{cat} and K_m values of the *Thermosipho africanus* TCF52 B (*TaCDP*) for celotriose were reported as 0.28 s⁻¹ and 0.094 mM, respectively (53). Compared to *BpGH94*_{MLG}, low phosphorolysis kinetic efficiency was

Utilizing mixed-linkage β -glucans by the *Blautia producta*

Table 3

Kinetic parameters of oligosaccharides phosphorolytic reaction by *BpGH94_{MLG}* compared with previously calculated kinetic parameters (*) of known CDPs, such as *Thermosipho africanus* TCF52B (*TaCDP*) (53); *Ruminiclostridium thermocellum* YM4 (*RtCDP*) (54), and *Ruminococcus albus* (*RaCDP*) (55)

Substrate	K_m (mM)	k_{cat} (s^{-1})	k_{cat}/K_m ($s^{-1} mM^{-1}$)	K_m (mM)	k_{cat} (s^{-1})	k_{cat}/K_m ($s^{-1} mM^{-1}$)	K_m (mM)	k_{cat} (s^{-1})	k_{cat}/K_m ($s^{-1} mM^{-1}$)	K_m (mM)	k_{cat} (s^{-1})	k_{cat}/K_m ($s^{-1} mM^{-1}$)
		<i>BpGH94_{MLG}</i>			<i>TaCDP</i> *			<i>Rt/CtCDP</i> *			<i>RaCDP</i> *	
Cellobiose		NA		0.120	0.23	1.1	0.81	NA		6.06	NA	
Celotriose	0.028 ± 0.004	0.67 ± 0.021	23.9	0.094	0.28	2.9		4	5		76.2	12.6
G4G3G	0.052 ± 0.005	1.86 ± 0.022	35.7		NA			NA			NA	
G4G4G3G	0.021 ± 0.002	1.21 ± 0.014	57.6		NA			NA			NA	

reported for the CDP of *Ruminiclostridium thermocellum* YM4, *RtCDP* (54), and *Ruminococcus albus*, *RaCDP* (55) (Figs. 5 and S2). None of these CDPs cleave cellobiose, but they can generate Glc-1-P from celotriose. They also accept β -(1,4)-linked glucans with DP ≥ 2 as acceptors for Glc-1-P-based synthesis (55, 56). Such actions were discrete from characterized β -(1,3)-glucan phosphorylases belonging to GH149, which work on acceptors with DP ≥ 1 (57). The phosphorolysis kinetic efficiency supports its role in the utilization of oligosaccharides derived from mixed linkage β -glucans.

The crystal structure of *BpGH94_{MLG}* was determined to a resolution of 2.3 Å (Table S1), revealing two copies of the protein molecules per asymmetric unit, forming a clear dimer (Fig. 5A). It contains a complex four-domain architecture, a β -sandwich domain extends into a smaller two α -helical linker domain connecting to an $(\alpha/\alpha)_6$ -barrel domain before terminating in a smaller β -sandwich domain (Fig. 5A). The top hit from a DALI analysis indicates a few close structural homologous in the PDB, giving Z scores in the range of 44.6 to 30.7 (58). For instance, chitobiose phosphorylase, ChBP, (PDB id-

1V7V/1V7W, Z scores 44.6), cellobiose phosphorylase, CBP (PDB ID- 2CQS, Z scores 43.4), laminaribiose phosphorylase, LBP (PDB ID- 6GGY, Z scores 32.6), and cellodextrin phosphorylase, *RtCDP* (PDB ID- 5NZ7/5NZ8, Z scores 30.7) shared 36%, 33%, 18%, and 23% sequence identify to *BpGH94_{MLG}*, respectively.

In contrast to *RtCDP* (Fig. 5B), *BpGH94_{MLG}* lacks an additional domain at the N-terminus end that is made up of mixed $\alpha\beta$ -structures (56). Although amino acid sequence similarities between *RtCDP*, ChBP, and CBP are limited, these can be structurally aligned with *BpGH94_{MLG}*. Structural alignment with *RtCDP*, CBP, and ChBP suggested that the active site of *BpGH94_{MLG}* is present at one end of the $(\alpha/\alpha)_6$ -barrel of the catalytic domain (Fig. 5, C, E, and G). Similar to *RtCDP*, CBP, and ChBP, a conserved residue, Asp515, is expected to act as a general acid catalyst. Comparing these phosphorylases highlights that *BpGH94_{MLG}* has a Y653 residue corresponding to Y804, and Y653 of *RtCDP*, and CBP, respectively (Fig. 5, D and F). This tyrosine is replaced with valine (V631) in the ChBP, a crucial residue for determining

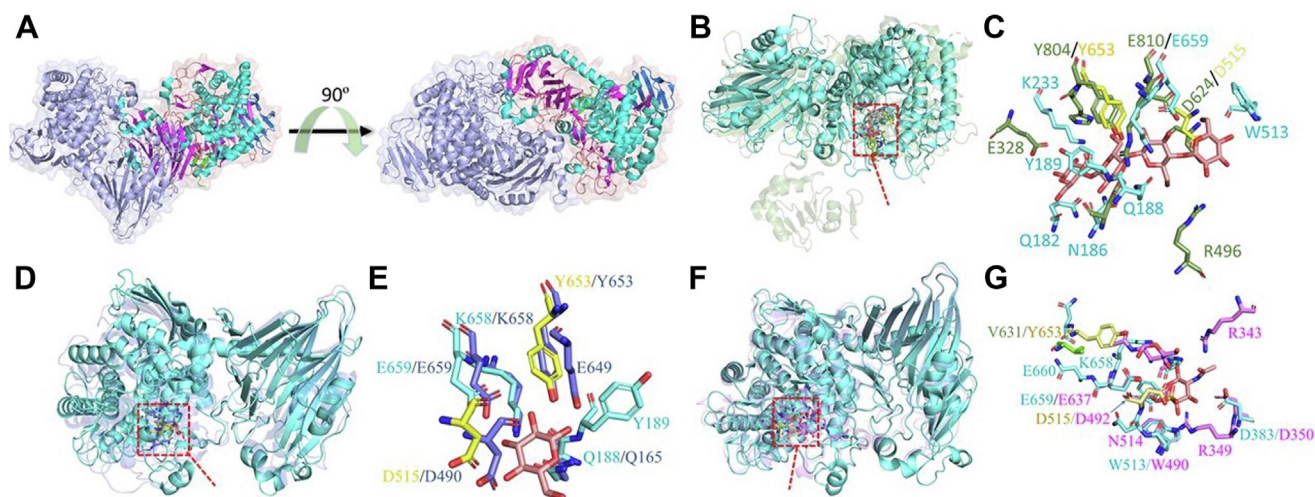


Figure 5. Crystal structure of *BpGH94_{MLG}* and comparison between other GH94. A, the crystal structure of *BpGH94_{MLG}* was determined to a resolution of 2.3 Å revealing two copies of the protein per asymmetric unit forming a clear dimer (N-terminal - green; loop- orange; α -helical- cyan; β -sheet- magenta; C-terminal- blue). B, superimposed *BpGH94_{MLG}* on celodextrin phosphorylase (PDB id: 5NZ8) and a red box highlighting catalytic domain (*BpGH94_{MLG}* - cyan and 5NZ8- green). C, identifying active residues of the *BpGH94_{MLG}* by comparing residues of the active site of 5NZ8 present around ligand (cellotetraose) in 3 Å vicinity (*BpGH94_{MLG}* - cyan, 5NZ8- green, D515 and Y653 of *BpGH94_{MLG}* - yellow and ligand- red). D, superimposed *BpGH94_{MLG}* on cellobiose phosphorylase (PDB id: 2CQS), and a red box highlighting catalytic domain (*BpGH94_{MLG}* - cyan and 2CQS- blue). E, identifying active residues of the *BpGH94_{MLG}* by comparing residues of the active site of 2CQS present around ligand (glucose) in 3 Å vicinity (*BpGH94_{MLG}* - cyan, 2CQS- blue, D515 and Y653 of *BpGH94_{MLG}* - yellow and ligand- light red). F, superimposed *BpGH94_{MLG}* on chitobiose phosphorylase (PDB id: 1V7W), and a red box highlighting catalytic domain (*BpGH94_{MLG}* - cyan and 1V7W- magenta). G, identifying active residues of the *BpGH94_{MLG}* by comparing residues of the active site of 1V7W present around ligand (N-acetylglucosamine) in 3 Å vicinity (*BpGH94_{MLG}* - cyan, 1V7W- magenta, and ligand- light red). These structures were processed in PyMol software.

substrate specificity for chitobiose (59). The architecture of the active site pocket of *BpGH94*_{MLG} is very similar to *RtCDP*, further suggesting that this enzyme is suitable for cleaving β -(1,4) linkages. Furthermore, a comparison of the active pocket of *BpGH94*_{MLG} and other GH94 suggested that *BpGH94*_{MLG} has an open active site pocket when compared to ChBP and CBP for accommodating short and longer chain substrates, such as G4G3G and G4G4G3G (Fig. S16).

Cytoplasmic digestion of mixed-linkage oligosaccharides by glycoside hydrolases

The human gut is a very complex system where redundancy for expressing a similar type of enzyme within a bacterium is frequently observed for glycan utilization. Therefore, we performed a proteomic analysis in order to identify enzymes that may be involved in the utilization of oligosaccharides produced by *BpGH16*_{MLG}. Through proteomics, we identified two GH3s (*Bp4420/BpGH3-AR8*_{MLG} and *Bp8539/BpGH3-X62*_{MLG}) that were upregulated when *B. producta* was grown on barley β -glucan (Fig. 1D). Both enzymes contain no signal peptide when analyzed with SignalP, v. 4.0, suggesting that they are cytoplasm-localized. Amino acid sequences were analyzed with NCBI Conserved Domain, suggesting that AR8_{MLG} and X62_{MLG} belong to the GH3 family (34).

*BpGH3-AR8*_{MLG} and *BpGH3-X62*_{MLG} both showed maximum activity in a phosphate buffer of pH 7.4 at 37 °C using pNP- β -D-Glc as a substrate (Fig. S17). Both enzymes cleaved β -(1,4), β -(1,3), and β -(1,6)-linked glucose from various oligosaccharides, including G4G3G and G4G4G3G (Fig. S18), with very similar kinetics parameters for each of these oligosaccharides (Table 4 and Fig. S19). The K_m values of both enzymes increased with increasing DP of cello-oligosaccharides and MLG-oligosaccharide, while those parameters remained similar with increasing DP of laminari-oligosaccharides. TLC profiles of enzyme-degraded products demonstrated that both enzymes sequentially cleaved glucose from the non-reducing end of cello-oligosaccharides, laminari-oligosaccharides, and MLG-oligosaccharide (Figs. S20 and S21). Both enzymes showed somewhat higher catalytic efficiency than recently reported for the MLG-degrading *BoGH3*_{MLG} (8). For example, *BpGH3-AR8*_{MLG} and *BpGH3-X62*_{MLG} show k_{cat}/K_m 71 and 67, 73 and 73.6 s⁻¹ mM⁻¹ for G4G3G and G4G4G3G, as compared to k_{cat}/K_m 47.4 and 41.8 s⁻¹ mM⁻¹ for G4G3G and G4G4G3G for

*BoGH3*_{MLG}, respectively. *B. ovatus* producing *BoGH3*_{MLG} (BACOVA_02745) shared 27% sequence similarity with *BpGH3-X62*_{MLG} and *BpGH3-AR62*_{MLG}.

Bioinformatics analysis

The prevalence of orthologues of the six proteins encoded by *B. producta* MLG degradation locus was assessed in other bacteria. Homology searches of sequences available in the NCBI NR database with the criteria of having at least 75% query coverage with at least 30% sequence similarity for each of the six proteins are presented in Figure 6A. It is evident that the locus in question is widely found among different genera of the Lachnospiraceae family, such as *Roseburia* and *Clostridium* sp. Furthermore, we identified homologues but variable similarity of all the six proteins in some species of *Butyrivibrio* sp., *Bacterium* D16-59, *Bacterium* D16-36, *Agathobacter* sp., *Candidatus Mediterraneibacter intestinigallinarum*, *Cellulosilyticum* sp., *Coprococcus* sp., *Dorea* sp., *Eubacterium uniforme*, *Eubacterium* sp. MSL-33, *Eubacteriales*, *Roseburia* sp., and *Treponema* sp. (Fig. 6A). *Blautia pseudococcoides* has homologs with ~90% sequence similarity for five proteins and 67% query coverage with AraC family protein. The comparative analysis revealed that a total of 37 out of 62 species have homologs of all six proteins. Interestingly, *BpSBP*_{MLG} and *BpGH94*_{MLG} in many bacteria showed high sequence identities, suggesting that members of Lachnospiraceae are evolutionarily adapted to utilize MLG oligosaccharides in order to survive in the nutrient-competitive environment of the gut.

Utilization of *BpGH16*_{MLG}-released oligosaccharides by other beneficial bacteria

We next investigated the importance of *BpGH16*_{MLG} in supporting the growth of human gut-beneficial bacteria on oligosaccharides generated from barley β -glucan. Some human gut Gram-positive bacteria belonging to the Lachnospiraceae were used for this analysis as it was observed from bioinformatic analysis that the locus of *B. producta* has a commonality with these bacteria. As a representative of commonality and other members of Lachnospiraceae, we selected *Roseburia faecis* JCM 17581^T/M72, and *Blautia coccooides* JCM 1395^T and *Anaerostipes caccae* JCM 13470^T, respectively. Additionally, we used species of *Bifidobacterium*

Table 4
Kinetics parameters for hydrolyzing various natural substrates by *BpGH3-AR8*_{MLG} and *BpGH3-X62*_{MLG}

Substrate	Kinetics parameters for <i>BpGH3-AR8</i> _{MLG}			Kinetics parameters for <i>BpGH3-X62</i> _{MLG}		
	K_m (mM)	k_{cat} (s ⁻¹)	k_{cat}/K_m (s ⁻¹ mM ⁻¹) PAHBAH assay	K_m (mM)	k_{cat} (s ⁻¹)	k_{cat}/K_m (s ⁻¹ mM ⁻¹) PAHBAH assay
G4G3G	0.24 ± 0.04	17 ± 0.3	71	0.23 ± 0.04	17 ± 0.3	73
G4G4G3G	0.3 ± 0.04	20 ± 0.3	67	0.25 ± 0.05	18 ± 0.3	74
Cellobiose	0.20 ± 0.03	8 ± 0.1	37	0.2 ± 0.03	8 ± 0.01	38
Cellotriose	0.26 ± 0.03	15 ± 0.2	58	0.26 ± 0.03	15 ± 0.2	59
Cellotetraose	0.47 ± 0.06	20 ± 0.2	42	0.45 ± 0.06	19 ± 0.3	43
Laminaribiose	0.24 ± 0.03	12 ± 0.2	48	0.24 ± 0.02	12 ± 0.2	48
Laminaritriose	0.23 ± 0.05	12 ± 0.2	52	0.24 ± 0.04	12 ± 0.2	51
Gentiobiose	0.24 ± 0.04	14 ± 0.2	58	0.24 ± 0.03	14 ± 0.2	58

Blanks were applied to all reaction mixtures (substrate and buffer without enzyme) and processed similarly to test samples. The blank value was subtracted from the test value in PAHBAH reducing sugar assay.

Abbreviation: PAHBAH, *p*-hydroxybenzoic acid hydrazide.

Utilizing mixed-linkage β -glucans by the *Blautia producta*

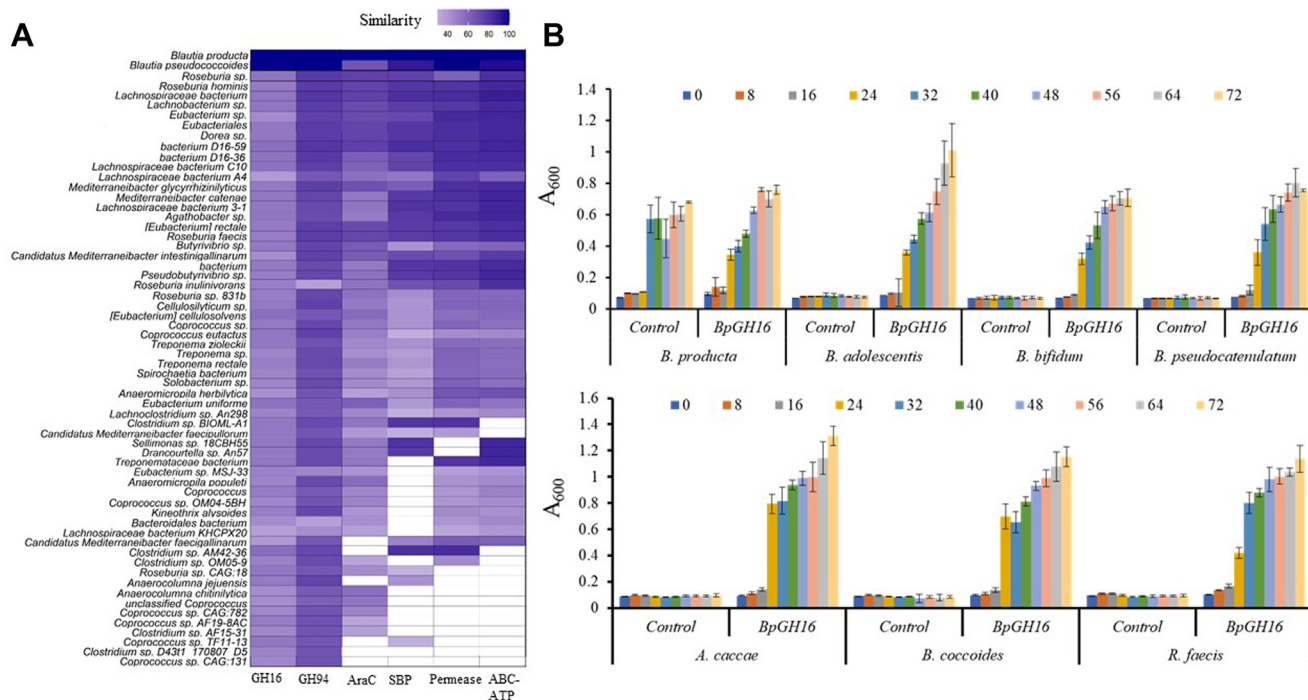


Figure 6. Prevalence of barley β -glucan utilizing locus across human gut microbiota and Growth patterns of some human gut bacteria. A, prevalence of all the six proteins of *B. producta* shown by histogram. The X-axis includes all six proteins and Y-axis includes all species identified from the sequence homology searches. The color of each rectangular for each member is corresponding to the percentage similarity. The image generated using the R script was further rearranged manually based on protein occurrence and similarity. B, growth patterns of different human gut bacteria on barley β -glucan. Bacteria were grown on a minimal medium containing 1% barley β -glucan in the absence or presence of BpGH16_{MLG}. Growth patterns of all human gut bacteria were determined in a period of 72 h, and growth was measured in an alternative of 8 h spectrophotometrically. *B. producta* only grew on a minimal medium containing 1% barley β -glucan in the absence of BpGH16_{MLG}, while other bacterial strains showed dependency on BpGH16_{MLG} for generating oligosaccharides. The generated oligosaccharides seem to be appropriate carbon sources for all six selected strains.

(*Bifidobacterium pseudocatenulatum* JCM 1200^T, *Bifidobacterium adolescentis* JCM 1275^T, and *Bifidobacterium bifidum* JCM 1254) that are commonly associated with health promotion (60, 61). All selected bacterial members started to grow and reached the stationary phase after 16 h and 56 h of incubation. Overall, all members showed robust growth on oligosaccharides generated by BpGH16_{MLG} from barley β -glucan and compared to the parent polysaccharide (Fig. 6B). Only *B. producta* showed growth on barley β -glucan (Fig. 6B) as compared to other bacteria (Fig. 6B). We visited the genomes of these selected strains where *R. faecis* showed 40 to 62% protein sequence similarity with locus-encoded genes (Fig. 6A). Despite having these sequence similarities, the strain could not grow on a minimal medium with 1% barley β -glucan, suggesting that *R. faecis* encoded GH16 may have different functional properties. *B. pseudocatenulatum* JCM 1200^T has 40% (gene id 2562617145) and 46% (gene id 2563201727) homolog with BpGH3-X62_{MLG} and BpGH3-AR62_{MLG}, respectively. *B. adolescentis* JCM 1275^T has 41% (gene id 639633010) and 47% (gene id 639764571) homolog with BpGH3-X62_{MLG} and BpGH3-AR62_{MLG}, respectively. *B. coccoides* JCM 1395^T showed protein sequence similarity with 99% (gene id 2799456949 and 2799455541 with BpGH3-X62_{MLG} and BpGH3-AR62_{MLG}, respectively). *B. bifidum* JCM 1254 and *A. caccae* JCM 13470^T do not have homologous MLG utilization proteins to *B. producta* but possess β -glucosidases belonging to the GH1, GH2 and GH3 families.

Since *B. producta* grew on barley β -glucan, it was thought that it can produce short-chain fatty acids (SCFAs) after fermenting digested barley β -glucan. Thus, they were grown in 96 well plates containing minimal medium with 1% barley β -glucan, and produced SCFAs from culture supernatant were measured through HPLC. Peaks were confirmed by the retention time of standards. Acetate, propionate, and butyrate were present in the culture supernatant in the ratio of 6.5:2.5:1, respectively (Fig. S22). In general, acetate, propionate, and butyrate are present in a molar ratio of 60:20:20 in the GIT, accounting for >95% of the SCFA content (62). However, this ratio varies based on the carbon source available to microbial communities (63).

Discussion

Gram-negative bacteria, such as *B. ovatus* ATCC 8483, encode all necessary genes for MLG-utilization in a single locus, including those for periplasmic utilization of released and imported oligosaccharides (8). In contrast, in Gram-positive bacteria such as *B. producta* and other strains only some of the necessary genes for MLG utilization are co-located (Fig. 6A). The gpPUL lacks the SusC and SusD proteins as present on the Gram-negative PULs paradigm. The gpPUL also deprives of SGBP (as it is present in Gram-negative bacteria, such as *B. ovatus* ATCC 8483) and a function of SGBP is often replaced by a CBM, associated with endoacting GHs

linked to gpPULs (26, 27). The present study further extends the finding of Sheridan *et al.* (26), who predominantly identified the gpPULs in *Roseburia/E. rectale* pangenome, by virtue of identifying gpPUL in various genera of Gram-positive bacteria (6A). As per definition of gpPUL, *B. producta* MLG-PUL consisted of a transcriptional regulator, one polysaccharide-degrading enzyme and a carbohydrate transport system.

Similar to *BoGH16_{MLG}* (8) and other organisms with PULs associated GH16s (23, 31, 64), *BpGH16_{MLG}* is present on the outer cell membrane and cleaves different structural types of β -glucans (Fig. 7). When fed barley MLG, *BpGH16_{MLG}* produces G4G3G and G4G4G3G as limit digest products, as does the corresponding *B. ovatus* enzyme, *BoGH16_{MLG}*. SGBP provides an access for barley MLG to *BoGH16_{MLG}* (~30 kDa). In the case of Gram-positive bacteria, CBM4 domains are known to bind β -(1,3) and β -(1,3/4) glucans (65). Therefore, four CBM4 domains of *BpGH16_{MLG}* may collectively offer an advantage for binding solid plant material in the gut environment.

BpSBP_{MLG} is identified as a bespoke transporter to trap β -(1,3)- and β -(1,4)-linked oligosaccharides in a gut environment. Mannan-binding SBP (*RiMnBP*) of *Roseburia intestinalis* has been reported to bind mannan-derived oligosaccharides at μ M levels (27). The primary parameters influencing the selective absorption of oligosaccharides by Gram-positive bacteria are SBPs of ABC transporters (46, 66, 67). The ABC transporter of *Roseburia inulinivorans* was previously observed to overexpress by about ten fold in the

presence of inulin as compared to fructose (68). *RiMnBP* was approximately overexpressed by sixfold in the presence of konjac glucomannan and spruce acetylated galactoglucomannan (AcGGM) when compared to glucose in transcriptomic analysis (27). *RiMnBP* was highly abundant (34-fold) in proteomic data of AcGGM grown culture of *R. intestinalis*. In line with these previous studies, *BpSBP_{MLG}* was highly abundant in proteomic data -76-fold higher in barley β -glucan grown *B. producta* culture as compared to glucose grown culture. The importance of *BpSBP_{MLG}* was confirmed by genetic deletion, where the mutant bacterium showed retarded growth on barley β -glucan.

Further, the oligosaccharide specificity of *BpSBP_{MLG}* is aligned with cytoplasmic *BpGH94_{MLG}* and GH3 (*BpGH3-AR8_{MLG}* and *BpGH3-X62_{MLG}*). It highlights that *B. producta* ATCC 27340 can employ two distinct mechanisms (Fig. 7) given that *BpGH94_{MLG}*, *BpGH3-AR8_{MLG}* and *BpGH3-X62_{MLG}* have approximately similar kinetic efficiencies for utilizing MLG-derived oligosaccharides (Tables 3 and 4; Fig. 5). In the first pathway, *BpGH94_{MLG}* phosphorolytically cleaves β -(1,4)-linked oligosaccharides in the cytoplasm and produces cellobiose, laminaribiose and Glc-1-P as final products from G4G3G and G4G4G3G (Fig. 7). The resulting Glc-1-P directly enters into glycolysis, saving a molecule of one ATP overall. Alternatively, imported oligosaccharides can be hydrolyzed to monosaccharides by *BpGH3-AR8_{MLG}* and *BpGH3-X62_{MLG}*, forming a second efficient pathway (Fig. 7). Orthologues of *BpGH3-AR8_{MLG}* and *BpGH3-X62_{MLG}* were observed in our previous

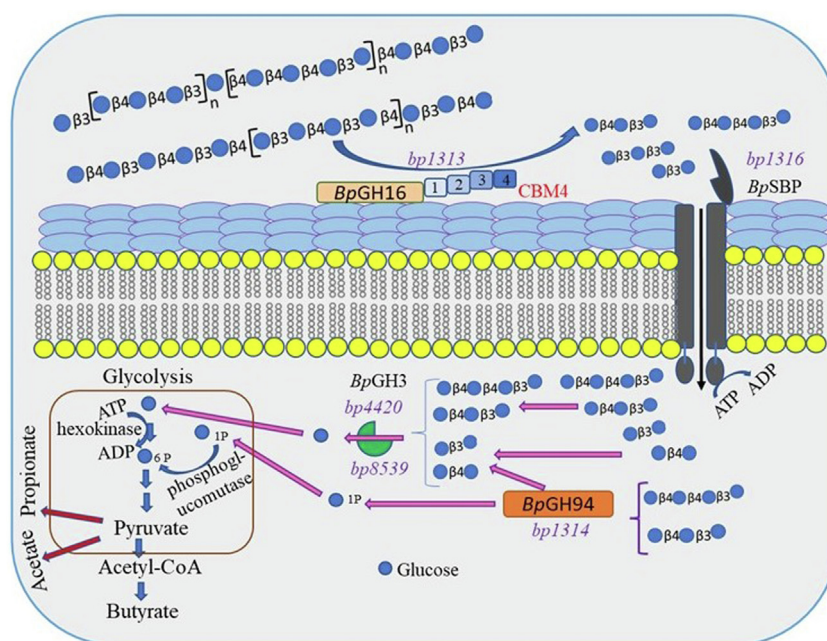


Figure 7. Overall digestion of barley β -glucan and lichenan by the *B. producta*. The *BpGH16_{MLG}* digests barley β -glucan and lichenan in the gut environment and releases various oligosaccharides. The resulting oligosaccharides are sensed by *BpSBP_{MLG}* and transported into the cytoplasm by ABC transporter component expressed by the locus. Imported oligosaccharides can be processed through *BpGH94_{MLG}*. Biochemical and crystal investigations suggested that *BpGH94_{MLG}* produced disaccharides and α -D-Glc-1-P as limit digest products from imported oligosaccharides. Proteomics analysis on barley β -glucan grown *B. producta* culture identified *BpGH3-AR8_{MLG}* and *BpGH3-X62_{MLG}*. This analysis suggested that those generated disaccharides or/and imported mixed-linkage oligosaccharides can be digested by *BpGH3-AR8_{MLG}* and *BpGH3-X62_{MLG}* and converted into glucose. Biochemical analyses revealed that these enzymes are highly efficient in utilizing β -(1,3), (1,4), and (1,6) linked oligosaccharides. Produced glucose and glucose-1 phosphate enter into metabolic pathways that ferment into acetate, butyrate, and propionate. These SCFAs are analyzed by HPLC using a Hi-Plex H column (300 \times 7.7 mm; 8 μ m particle size, Agilent Tech).

Utilizing mixed-linkage β -glucans by the *Blautia producta*

work relating to the utilization of mixed linkage β -glucans in *Bacteroides uniformis* JCM 13288 (69).

Previously, Biddle, Stewart, Blanchard, and Leschine (70) performed a survey of the fibrinolytic potential among Lachnospiraceae and found the presence of various CAZymes families, CBM and ABC transporters for degrading pectin and hemicellulose. Indeed, our bioinformatic analysis highlights that barley β -glucan utilizing capability is prevalent among Lachnospiraceae and *Treponema* in the HGM (Fig. 6A). In particular, homologs of *BpGH94*_{MLG} and *BpSBP*_{MLG} are commonly present among members of Lachnospiraceae, the most abundant family of *Firmicutes* in the human colon, suggesting that they are evolutionarily adapted to use oligosaccharides generated in the gut environment.

We further explored the possible roles of *BpGH16*_{MLG} in cross-feeding systems with different glucans. We indeed demonstrated that oligosaccharides generated from barley β -glucan supported the growth of beneficial human gut bacterial species (Fig. 6B), which are normally associated with a healthy gut (71). For instance, *Bifidobacteria* demonstrate the ability to prevent and/or treat colorectal cancer and inflammatory bowel disease (61), while *B. bifidum* or *B. adolescentis* are known to alleviate low blood glucose concentration and gut microbiota disorders (72, 73) and the adult-dominant species *B. pseudocatenulatum* may prevent type 2 diabetes (74, 75). *B. coccoides* JCM1395^T is recently suggested to be used for tumor-targeted live bacterial therapeutics (76). Bacterial metabolites such as SCFAs are essential nutrients for human survival and mitigating various diseases in the human gut, including inflammatory bowel diseases (77). *Roseburia* species belong to butyrate-producing bacteria and can ameliorate alcoholic fatty liver (78). *A. caccae* has been recognized as butyrate-producing bacteria (79), thus enhancing the production of butyrate. Similarly, *B. producta* ATCC 27340 produces acetate, propionate, and butyrate, suggesting that the strain not only supports beneficial bacteria growth through a cross-feeding system but also promotes the health status of the host through producing SCFAs. Together with our observations, this suggests that *BpGH16*_{MLG} and *B. producta* itself have the potential to support the growth of beneficial bacteria *in vivo*, thus improving human health.

Although MLG positively affects microbial composition by increasing specific bacterial populations and maintaining gut-bacterial homeostasis for healthy individuals (80), much less is known about how beneficial bacteria utilize MLG at the molecular level. The GIT harbors a multifaceted and dynamic population of microorganisms that exert a significant effect on human health. The diet strongly influences the composition of the colonic microbiota and the balance of its metabolic products. Thus, diet presents promising opportunities for maintaining HGM homeostasis and preventing non-communicable diseases (81). In particular, genes of bacterial communities encode highly diverse enzymes for utilizing dietary glycans and act as a secondary genome of the host. A better understanding of the molecular mechanisms supported by these genes offers novel opportunities for intervention to address the dysbiosis of the HGM and prevent associated

chronic disorders. Gram-positive bacteria are under-explored in this regard. Herein, we have addressed this gap through a detailed analysis of *B. producta* ATCC 27340 MLG metabolism.

Experimental procedures

Lichenan from Icelandic moss, barley β -glucan, laminaribiose, laminaritriose, laminaritetraose, laminaripentaose, celotriose, cellobiosyl- β -D-1,3-glucose (G4G3G) were purchased from Megazyme, Ireland. Gentiobiose and laminarin were purchased from Sigma Aldrich. All NMR analyses were performed at Panjab University, Chandigarh, India. All kinetic parameters were performed with GraphPad Prism.

Assessment bacterial growth on β -glucans

Active culture of *B. producta* and culture conditions were maintained following the recently reported procedure (31). Once *B. producta* grew, cells were centrifuged, and the obtained supernatant was decanted. A pellet of cells was then washed three times with phosphate-buffered saline (PBS) and washed cells were suspended in 2 ml PBS. 5 μ l of cell suspended volume was inoculated in 200 μ l of minimal medium containing 1% barley β -glucan or lichenan on 96 well plates. The growth assessment experiments were performed for 96 h, following our recently established protocol (82).

Total RNA extraction and gene expression analysis

Changes in the transcript expression levels of the β -glucan utilization locus of *B. producta* were performed by RT-qPCR. *B. producta* was initially cultured in 5 ml of GAM for 24 h and cells were spun down by centrifugation and washed three times with sterile PBS. Afterward, 20 μ l of 1 ml suspension of bacterial cells was cultured in a 10 ml minimal medium containing 1% (w/v) barley β -glucan, 3 ml of bacterial cultures were collected at mid-log phase (A600 about 0.6) by centrifugation at 15,000g and resuspended in 300 μ l of a solution consisting of 1 mM EDTA, 0.5% SDS and 0.02 M sodium acetate (pH 5.5). Immediately, 300 μ l saturated phenol with citrate buffer (pH 4.3, P4682- Sigma Aldrich) was added, and the mixed solution was incubated at 60 °C for 5 min with mild shaking. After that, it was centrifuged at 15,000 g for 5 min, and the upper aqueous phase was transferred into a new Eppendorf tube. It was mixed with three volumes of chilled ethanol and incubated for 30 min at -80 °C. The precipitate was then collected by centrifugation at the same speed, the pellet was washed with 70% ethanol twice, and the final white residue was dissolved in 100 to 500 μ l of distilled water. The concentration of total RNA was calculated by a spectrophotometer at 260 nm. If a residual amount of DNA was observed, DNase-1 treatment was also given, following the manufacturer's instructions (AMPD1, Sigma Aldrich).

About 2 μ g total RNA was immediately used for reverse transcription using AccuScript High Fidelity cDNA Synthesis Kit (Agilent). RT-qPCR was performed in a 96-well plate on a CFX96 qPCR system (BioRad) using SYBR Green Master (BioRad), using the primers mentioned in Table S2. The qPCR

reactions were executed in 10 μ l, consisting of 5 μ l of SYBR green mix, 30 ng of cDNA, and one pmol of each primer of a gene of the locus or 16S rRNA (Table S2). The reaction condition was 95 °C for 10 min, followed by 40 cycles of 95 °C for 10 s, 55 °C for 10 s, and 72 °C for 10 s. The $2^{-\Delta\Delta C_t}$ method calculated the expression of each gene and normalized data to 16S rRNA transcript level. Finally, the expression level of each gene was calculated as fold change compared with cultures of a minimal medium containing 1% glucose. Three technical replicates were used for bar generation of each gene expression; each bar represents average values and error bars indicate the standard errors of three technical replicates.

Proteomics

B. producta ATCC 27340 was anaerobically grown at 37 °C overnight, cells were collected by centrifugation (3000g at room temperature, RT) and washed thrice with 5 ml PBS. After that, cells were resuspended into 2 ml PBS and 5 μ l of it was inoculated into filtrated (0.2 μ m filters) 10 ml minimal medium containing 1% barley β -glucan or glucose. The strain was grown to the mid-late exponential phase ($A_{595} \sim 0.5$ – 0.6) in two biological replicates. Cells were collected by centrifugation (5000g) for 5 min at 4 °C, washed twice with ice-cold PBS, and resuspended in a 2 ml lysis buffer (50 mM HEPES containing protease inhibitors, pH 6.5). For proteome analysis, cells were lysed by a bead beater (three cycles of 60 s on MP Biomedicals, CA) using glass beads (acid washed ≤ 106 μ m). The lysate was centrifuged (15,000g, 15 min at 4 °C), and the supernatant was collected. Procedures for the precipitation of protein, trypsin digestion, and analysis of generated peptides have been mentioned in the Supplementary file.

Cloning of identified genes and recombinant production of the corresponding enzymes

A predicted β -glucan utilization locus of *B. producta* was identified from the genome (33), and genes of the locus were retrieved based on gene ID- 2515951313 to 2515951318 of IMG genome ID- 2515154176 using the Integrated Microbial Genomes (IMG) and Metagenomes (IMG/M) portal. Cellular location based on the signal peptide of proteins encoded by β -glucan utilization locus was predicted using SignalP, v. 4.0 online server (36). Subsequently, appropriate primers were designed (Table S3) after excluding lipidated and signal peptide sequences. The lipidated amino acid of a protein was screened with the LipoP 1.0 server (35). Restriction sites of primers were wisely selected after investigating that no restriction sites of selected restriction enzymes were present within the gene. As previously reported, the amplification of genes was achieved by PCR, and products were purified (31). Then, purified PCR products were cloned into pET28a(+) plasmid, having N-terminal (His)₆-tag. Cloned constructs were transformed into *E. coli* TOP10 cells. Screening for positive clones and plasmid preparation was performed. After checking the genetic integrity of all clones, cloned constructs were transformed into *E. coli* BL21 (DE3) for expression of proteins. Genes of ID- 2515951313 and ID- 2515951314 were

synthesized and inserted into pET28a(+) by the GenScript Biotech PTE.LTD

Expression and purification of enzymes

E. coli BL21 cells were cultured in the Terrific broth (TB) (for *BpGH16_{MLG}*) or Luria-Bertani (LB) medium (for all other proteins) containing kanamycin (50 μ g/ml) to absorption ~ 1.2 or mid-log phase (A_{600} nm of ~ 0.6) at 37 °C respectively. Afterward, the expression of proteins was induced by adding 0.4 or 0.5 mM isopropyl β -D-1-thiogalactopyranoside (IPTG) to bacterial cultures. LB medium was further incubated at 22 °C for 16 h. In the case of the TB medium, the protein was induced by incubating at 18 °C for 16 h. Post incubation, bacterial cells were harvested by spinning at 4000g and then resuspended in 50 mM HEPES buffer (pH 7.5) with an appropriate EDTA-free protease inhibitor cocktail (Sigma Aldrich, Cat. No. 4693159001). Cells were lysed by ultrasonication, and the supernatant was then obtained by centrifugation at 16,000g for 30 min at 4 °C. Obtained supernatant was initially concentrated through Amicon Ultra-15 Centrifugal Filter Unit (10 kDa, Merck). It was then mixed with 20 ml suspension of nickel-nitrilotriacetate (Ni-NTA) resin and incubated for 15 min at 4 °C. Followed by entire resin was filled in a column, and different gradients (10, 50, 100, 150, 200, and 500 mM) of imidazole containing 500 mM NaCl were applied in a column to get a purified form of a protein. Intended proteins were eluted in 50 to 150 mM imidazole, and imidazole was then replaced with 50 mM HEPES buffer (pH 6.5) by Amicon Ultra-15 Centrifugal Filter Unit (10 kDa). A 10% sodium dodecyl sulfate–polyacrylamide gel electrophoresis (SDS-PAGE) was performed to determine the desired protein's molecular weight (Fig. S23). A native-PAGE was also used to assess the dimerization of *BpGH94_{MLG}* (Fig. S24). The concentration of purified proteins was finally determined by a spectrophotometer using Bradford reagent, and all proteins were then stored at -80 °C till further analysis, having a final concentration of 1 mg/ml.

Site-directed mutagenesis

The residues R331, L358, E379, D381, E384, W362, and H398 of *BpGH16_{MLG}* were mutated to Ala by the Q5Site-Directed Mutagenesis Kit (New England Biolabs, UK, catalogue no. E0554S). Wild-type plasmid *BpGH16*-pET28a(+) was used as a template, and mutagenic forward and reverse primers were developed using NEBaseChanger with subtle modifications (Table S4). A 25 μ l PCR cocktail was prepared for mutating each residue. The final concentration of Q5 Hot Start High-Fidelity 2X Master Mix was 1X, each primer was at 0.5 μ M, the amount of used template was 20 ng, and the rest of the volume was made up of nuclease-free water. PCR was executed using the following conditions-initial denaturation was performed at 98 °C for 1 min, for each cycle-denaturation, annealing, and extension (72 °C) were set for 10 s, 20 s, and 7 min, respectively. A total of 25 cycles were performed, and the final extension was for 5 min 5 μ l PCR products were loaded on 0.8% agarose gel to conform to the amplification of

Utilizing mixed-linkage β -glucans by the *Blautia producta*

the mutagenic gene. Ligation of PCR products and cleavage of methylated template DNA was then performed using 5 μ l KLD reaction buffer and 1 μ l KLD enzyme cocktail at RT for 1 h. It was then transformed into *E. coli* TOP-10 cells and plasmids were isolated. The obtained plasmids were sequenced to confirm the mutation at the desired location. Once mutation was confirmed in a gene, the mutant plasmid was transformed into Rosetta (DE3) cells for protein expression. The mutant protein was then expressed as per the protocol mentioned earlier, and kinetics were performed with barley β -glucan.

Evaluating biochemical properties of enzymes

The optimum pH of *BpGH16*_{MLG}, *BpGH94*_{MLG}, *BpGH3-AR8*_{MLG}, and *BpGH3-X62*_{MLG} was accomplished in various buffers by incubating reactions at 37 °C for 15 min in a standard reaction mixture volume (100 μ l), consisting of 10 μ l of 10 mM substrate and recombinant enzyme at a final concentration of 0.1 mg/ml. *pNP*- β -laminaribioside, and *p*-nitrophenyl- β -D-glucopyranoside (*pNP*- β -Glc) were used as a substrate for *BpGH16*_{MLG} and *BpGH3-AR8*_{MLG}/*BpGH3-X62*_{MLG}, respectively. Different buffers of 50 mM concentration, such as citrate (pH 3–5.5), sodium phosphate (pH 5.7–8), sodium acetate (pH 4–6), Tris-HCl (pH 7–9), and HEPES (pH to 5.1–9) were used. All reactions were terminated by adding 6 volumes of 1 M Na₂CO₃. The released amount of *p*-nitrophenol was determined by measuring the absorbance at 410 nm using NUNC 96 well plates on the SpectraMax i3x multi-mode microplate reader. The concentration of released *p*-nitrophenol was calculated accordingly to Beer Lambert law ($A = \epsilon cl$, where ϵ is the molar extinction coefficient of *p*-nitrophenol at 410 nm, c is the concentration and l is the optical path length in cm) as reported previously (83).

A reaction mixture consisting of 10 μ l Glc-1-P (100 mM), recombinant enzyme (final concentration at 0.1 mg/ml), 10 μ l cellobiose (100 mM), and 20 μ l sodium molybdate (1 M) was used for determining optimum pH for *BpGH94*_{MLG}. For determining the optimal temperature of *BpGH94*_{MLG}, a reaction mixture consisting of 10 μ l Glc-1-P (100 mM), recombinant enzyme (final concentration at 0.1 mg/ml), 10 μ l cellobiose (100 mM), 20 μ l sodium molybdate (1 M), was incubated at 15, 22, 30, 37, 45 and 55 °C for 30 min. Then, 25 μ l of the reaction mixture was mixed with 75 μ l of a color solution (0.24% [w/v] sodium ascorbate dissolved in 0.1 N HCl solution), and it was incubated at RT until color developed. Once the color was developed, the reaction was terminated by adding 75 μ l stop solution (2% [w/v] sodium citrate tribasic dihydrate in 2% [v/v] acetic acid). Released inorganic phosphate concentration was determined by determining color absorbance at 620 nm using NUNC 96 well plates. A phosphate release assay was used to measure released inorganic phosphate (84). A standard curve of KH₂PO₄ (0–2.5 mM) was made to determine the released amount of inorganic phosphate upon enzymatic reactions.

For determining the optimal temperature of *BpGH16*_{MLG}, standard reactions (100 μ l) having recombinant enzyme (final concentration at 0.1 mg/ml) and 10 μ l of 10 mM *pNP*- β -

laminaribioside were performed at different temperatures (15, 22, 30, 37, 45 and 55 °C) for 15 min using optimized pH. For determining the optimal temperature of *BpGH3-AR8*_{MLG} and *BpGH3-X62*_{MLG}, standard reactions (100 μ l) having recombinant enzyme (final concentration at 0.1 mg/ml) and 10 μ l of 10 mM *pNP*- β -Glc were performed at different temperatures (15, 20, 25, 30, 37, 42, 48 and 55 °C) for 30 min using optimized pH.

Initial screening of *BpGH16*_{MLG} was performed in 100 μ l reaction volume containing 10 μ l of 10 mM of various oligosaccharides (such as sucrose, maltose, gentiobiose, cellobiose, celotriose, laminaribiose, laminaritriose, laminaripentaose, and G4G3G) and 10 μ l of 10 mg of various polysaccharides (laminarin, lichenan, lentinan, oat β glucan, and barley β -glucan) and recombinant enzyme (final concentration at 0.1 mg/ml) in optimized buffer (pH 5.7) for 2 h at 37 °C. After the appropriate incubation time, the reaction was terminated by boiling (5 min), and generated oligosaccharides were analyzed by thin layer chromatography (TLC). Typically, 1 μ l of the reaction mixture was used for TLC analysis. TLC analysis was performed on Silica Gel 60 F254 (Merck), and produced sugars were visualized by spraying TLC with 5% H₂SO₄ in ethanol, followed by heating. For determining limit digest products of laminarin, barley β -glucan, and lichenan by the action of the *BpGH16*_{MLG}, reactions were executed at different intervals (2, 4, 8, and 24 h), and products were analyzed by TLC and the matrix-assisted laser desorption ionization time-of-flight mass spectrometry (MALDI-TOF-MS).

Michaelis–Menten kinetic parameters (K_m , V_{max} , and k_{cat}) of the *BpGH16*_{MLG} were determined using a range of concentrations (0–1 mg/ml) of a substrate, such as laminarin, lichenan, oat β -glucan, and barley β -glucan. Reactions were performed in 100 μ l volume mixture using recombinant enzyme (final concentration at 0.1 mg/ml) in 50 mM sodium phosphate buffer (pH 5.7) at 37 °C for 1 h of incubation. Then, reactions were terminated by boiling for 5 min. Enzymatic assays were determined with 3,5- dinitrosalicylic acid (DNS) assay (85). In brief, 0.05 g Na₂SO₃ and 1 g DNS were mixed in a 50 ml water-containing reagent bottle and stirred about 6 h using a magnetic stirrer. After that, 200 μ l phenol was added and made up to 100 ml. A working solution of DNS was prepared by adding 50 μ l glucose (20% (w/v) stock) in prepared 100 ml of reagent mixtures and immediately used for experiments without adding NaOH. 80 μ l DNS reagent was added to the reaction mixtures and incubated at 100 °C for 10 min, followed by ice-cooling for 10 min. Consequently, recorded the developed color spectrophotometrically at 575 nm (85). A standard curve generated by different concentrations of maltose was used for determining released reducing sugars in each case.

The phosphorolysis activity of *BpGH94*_{MLG} was determined with various oligosaccharides and MLG (barley β -glucan and lichenan) at the concentration of 10 mM using 100 mM inorganic phosphate and recombinant enzyme (final concentration at 0.2 mg/ml) in 100 mM HEPES buffer (pH 6.5) at 37 °C and various incubation time (2, 4, 8, or 20 h). TLC was

used for analyzing enzymatic actions. MALDI-TOF-MS determined the limit-digest products of barley β -glucan and lichenan with *BpGH94_{MLG}*. Kinetics parameters for *BpGH94_{MLG}* were determined with G4G3G, G4G4G3G and celotriose, following a *p*-hydroxybenzoic acid hydrazide (PAHBAH) reducing sugar assay (69).

Kinetics parameters for *BpGH3-AR8_{MLG}* and *BpGH3-X62_{MLG}* were also determined with natural oligosaccharides, such as cellobiose, celotriose, cellotetraose, laminaribiose, laminaritriose, gentiobiose, G4G3G and G4G4G3G. Recently reported PAHBAH reducing sugar assay used for kinetic parameters of these enzymes (69). In brief, different concentrations of these oligosaccharides (2 μ M–1 mM) were incubated with recombinant *BpGH3-AR8_{MLG}* and *BpGH3-X62_{MLG}* (final concentration at 0.1 mg/ml) for 5 to 30 min in 100 mM HEPES buffer (pH 6.5) at 37 °C. 150 μ l of a freshly prepared 8:2 mixture of reagent A (50 mM sodium sulfite, 0.3 M 4-hydroxybenzhydrazide and 0.6 M HCl) and reagent B (50 mM trisodium citrate, 10 mM CaCl₂, 0.5 M NaOH) were added to 50 μ l sample. The reaction cocktail was boiled for 10 min at 100 °C. After the reaction was cooled down, the absorbance was recorded at 410 nm using the SpectraMax i3x multi-mode microplate reader. A calibration curve with different concentrations of glucose (0, 2, 4, 8, 16, 40, 80, 100, 200, 300, and 500 μ M) was employed for each experiment to calculate the released amount of glucose (reducing end equivalents). The same samples were also used for control measurement, and the control value was subtracted from test reading prior to calculate kinetics parameters. In all cases, the K_m , V_{max} , and k_{cat} were analyzed on GraphPad Prism. Three independent replicates were used for each test. TLC analyses were used for understanding the enzymatic degradation profiles of various oligosaccharides.

NMR analysis of limit-digest products of *BpGH16_{MLG}*

Barley β -glucan limit digest products of *BpGH16_{MLG}* were analyzed with ¹³C-DEPT- NMR to confirm the type of linkages in their digested products. 200 mg barley β -glucan was digested by the *BpGH16_{MLG}* overnight at 37 °C. All generated products were purified with size exclusion chromatography using Toyopearl resin (HW-40) filled column (100 × 25 mm). All eluted products were checked with TLC for chromatographic patterns and were freeze-dried for analysis. NMR was performed on a Bruker Avance Neo 500 MHz spectrometer equipped with a broadband BBFO probe. Chemical shifts (δ) were defined in parts per million (ppm) in which the residual solvent signal was demarcated as a reference point for assigning sample peaks. The data processing and analysis were performed with the MestreNova software.

Circular dichroism spectroscopy

The secondary structure prediction of the solute binding protein (*BpSBP_{MLG}*) was made on a 410 model CD spectrometer (Biologic Science Instrument, AL X 300, MOS 500) using 1 ml cuvette with a 5 mm path length. For all measurements, the *BpSBP_{MLG}* was diluted to 5 μ M in a 10 mM

phosphate buffer (pH 7) having 150 mM KCl. Spectra were recorded from 200 to 260 nm at 25 °C. Temperature scans were recorded at a wavelength of 220 nm. Data were fitted to a 2-state unfolding model.

Isothermal titration calorimetry analysis

The binding of β -(1,4), β -(1,3), and MLG-oligosaccharides to *BpSBP_{MLG}* was measured at 25 °C in 10 mM sodium phosphate buffer (pH 7) using a MicroCal PEAQ-ITC (Malvern). The protein was extensively dialyzed against 10 mM sodium phosphate and all glycan ligands were also dissolved in the same buffer to minimize the heat of dilution. 13 injections of an oligosaccharide were titrated on *BpSBP_{MLG}* present in the sample cell. Various preliminary titration setups were tried by changing amounts of protein (5–100 μ M) and ligand (50 μ M–10 mM) to get the best experimental conditions. Thermodynamic binding parameters [calculates binding affinity (K_d), stoichiometry (n), enthalpy (ΔH), Gibbs free energy change (ΔG), and entropy (ΔS)] were determined using the MicroCal PEAQ-ITC analysis software.

Bioinformatic analysis

The six protein sequences of a barley- β -glucan utilizing locus belonging to *B. producta* were downloaded from JGI/IMG/M in fasta format: *BpGH16_{MLG}* (ID-2515951313), *BpGH94_{MLG}* (ID-2515951314), AraC family (ID-2515951315), *BpSBP_{MLG}* (ID-2515951316), ABC permease (ID-2515951317) and ABC ATP binding (ID-2515951318). To check the prevalence and identify homologs of these six proteins, we performed a BLAST sequence similarity search using NCBI BLAST (86). A detected homolog in different bacterial species was considered with the criteria of having at least 75% query coverage with at least 30% sequence similarity, and *BpGH16_{MLG}* and *BpGH94_{MLG}* should be present. Given that *BpGH16_{MLG}* shared 33% sequence similarity with *BoGH16_{MLG}* and both proteins were functional, these selection criteria were selected. All the output data was imported and filtered using in-house PERL and Shell scripts and sheets. The prevalence of hit distribution for all six proteins of a locus with similarity amongst all other species was plotted using a bubble plot in the R program using in-house scripts.

Growth of Gram-positive bacteria using exogenous *BpGH16_{MLG}*

R. faecis JCM 31261, *B. pseudocatenuatum* JCM 1200^T, *B. adolescentis* JCM 1275^T, *B. coccoides* JCM 1395^T, *B. bifidum* JCM 1254, and *A. caccae* JCM 13470^T were used for bacterial mono-culture experiments. All strains were maintained, and experiments were conducted under an anaerobic atmosphere consisting of 85% N₂, 10% CO₂, and 5% H₂ at 37 °C. About 5 μ l glycerol stock was initially inoculated to 5 ml of GAM for the primary culture of these strains. As soon as bacterial strains were grown, the cell pellet of each strain was separately obtained by centrifugation at 8000g for 1 min, and it was then washed three times with PBS. 5 μ l of dissolved cell suspension of pellets in PBS was inoculated into a 200 μ l minimal medium

Utilizing mixed-linkage β -glucans by the *Blautia producta*

containing 1% barley β -glucan in presence or absence of exogenous supply of *BpGH16*_{MLG} (0.05 mg/ml). The experiment was set up on 300 μ l flat-bottomed 96-well microtiter plates. Reading was taken every interval of 8 h at 600 nm on a spectrophotometer.

Data availability

Structure factors and atomic coordinates of *BpGH94*_{MLG} have been deposited with the Protein Data Bank with accession code; PDB ID 8BOU. All other data are provided either in the [Supporting information](#) or can be available from the corresponding author upon reasonable request.

Supporting information—This article contains supporting information (1, 3, 38, 39, 40, 48, 55, 83, 85, 87–93).

Acknowledgments—R. P. Singh would like to thank the Department of Biotechnology, India for providing the Ramalingaswami Re-entry Fellowship and Grant in-aid-number: BT/PR32876/PFN/20/1471/2020 and BT/PR38298/PFN/20/1558/2020. The authors would like to thank Dr Vikas Rishi from NABI, Mohali for assisting with circular dichroism (CD) spectroscopy analysis. The authors would like to thank the Diamond Light Source for beam-time on i03 (proposal mx24447-60). The University of Manchester is acknowledged for providing financial support.

Author contributions—R. P. S. conceptualization; R. P. S. and R. A. F. methodology; R. P. S., J. N., R. T., B. A. W., C. W. L., T. M., R. K., D. P., and G. K. investigation; R. P. S., J. N., and T. M. writing—original draft; R. P. S., T. M., and R. A. F. writing—review and editing.

Conflict of interest—The authors declare that they have no conflicts of interest with the contents of this article.

Abbreviations—The abbreviations used are: DP, degree of polymerizations; GAM, Gifu anaerobic medium; gpPUL, Gram-positive PUL; HGM, human gut microbiota; MLG, mixed linkage glucans; PUL, Polysaccharide Utilization Loci; SGBP, surface glycan-binding protein.

References

- Zhang, H., and Row, K. H. (2015) Extraction and separation of polysaccharides from *Laminaria japonica* by size-exclusion chromatography. *J. Chromatogr. Sci.* **53**, 498–502
- Chotigavin, N., Sripochanart, W., Yaiyen, S., and Kudan, S. (2021) Increasing the production of beta-glucan from *Saccharomyces carlsbergensis* RU01 by using tannic acid. *Appl. Biochem. Biotechnol.* **193**, 2591–2601
- Aman, P., and Graham, H. (1987) Mixed-linked beta-(1,3), (1,4)-D-glucans in the cell walls of barley and oats—chemistry and nutrition. *Scand. J. Gastroenterol. Suppl.* **129**, 42–51
- Harada, T., Misaki, A., and Saito, H. (1968) Curdlan: a bacterial gel-forming beta-1,3-glucan. *Arch. Biochem. Biophys.* **124**, 292–298
- Han, B., Baruah, K., Cox, E., Vanrompay, D., and Bossier, P. (2020) Structure-functional activity relationship of beta-glucans from the perspective of immunomodulation: a mini-review. *Front. Immunol.* **11**, 658
- Mejia, S. M. V., de Francisco, A., and Bohrer, B. (2020) A comprehensive review on cereal beta-glucan: extraction, characterization, causes of degradation, and food application. *Crit. Rev. Food Sci. Nutr.* **60**, 3693–3704
- Chen, J., and Raymond, K. (2008) Beta-glucans in the treatment of diabetes and associated cardiovascular risks. *Vasc. Health Risk Manag.* **4**, 1265–1272
- Tamura, K., Hemsworth, G. R., Dejean, G., Rogers, T. E., Pudlo, N. A., Urs, K., et al. (2017) Molecular mechanism by which prominent human gut *Bacteroidetes* utilize mixed-linkage beta-glucans, major health-promoting cereal polysaccharides. *Cell Rep.* **21**, 2030
- Drula, E., Garron, M. L., Dogan, S., Lombard, V., Henrissat, B., and Terrapon, N. (2022) The carbohydrate-active enzyme database: functions and literature. *Nucleic Acids Res.* **50**, D571–D577
- El Kaoutari, A., Armougom, F., Gordon, J. I., Raoult, D., and Henrissat, B. (2013) The abundance and variety of carbohydrate-active enzymes in the human gut microbiota. *Nat. Rev. Microbiol.* **11**, 497–504
- Jayachandran, M., Chen, J., Chung, S. S. M., and Xu, B. (2018) A critical review on the impacts of beta-glucans on gut microbiota and human health. *J. Nutr. Biochem.* **61**, 101–110
- Almeida, A., Mitchell, A. L., Boland, M., Forster, S. C., Gloor, G. B., Tarkowska, A., et al. (2019) A new genomic blueprint of the human gut microbiota. *Nature* **568**, 499–504
- Qin, J., Li, R., Raes, J., Arumugam, M., Burgdorf, K. S., Manichanh, C., et al. (2010) A human gut microbial gene catalogue established by metagenomic sequencing. *Nature* **464**, 59–65
- Rakoff-Nahoum, S., Foster, K. R., and Comstock, L. E. (2016) The evolution of cooperation within the gut microbiota. *Nature* **533**, 255–259
- Xu, J., Mahowald, M. A., Ley, R. E., Lozupone, C. A., Hamady, M., Martens, E. C., et al. (2007) Evolution of symbiotic bacteria in the distal human intestine. *PLoS Biol.* **5**, e156
- Terpend, K., Possemiers, S., Daguet, D., and Marzorati, M. (2013) Arabinogalactan and fructo-oligosaccharides have a different fermentation profile in the simulator of the human intestinal microbial ecosystem (SHIME (R)). *Environ. Microbiol. Rep.* **5**, 595–603
- Daguet, D., Pinheiro, I., Verhelst, A., Possemiers, S., and M, M. (2016) Arabinogalactan and fructooligosaccharides improve the gut barrier function in distinct areas of the colon in the simulator of the human intestinal microbial ecosystem. *J. Funct. Foods* **20**, 369–379
- Reichardt, N., Vollmer, M., Holtrop, G., Farquharson, F. M., Wefers, D., Bunzel, M., et al. (2018) Specific substrate-driven changes in human faecal microbiota composition contrast with functional redundancy in short-chain fatty acid production. *ISME J.* **12**, 610–622
- Frost, G., Sleeth, M. L., Sahuri-Arisoylu, M., Lizarbe, B., Cerdan, S., Brody, L., et al. (2014) The short-chain fatty acid acetate reduces appetite via a central homeostatic mechanism. *Nat. Commun.* **5**, 3611
- Francino, M. P. (2015) Antibiotics and the human gut microbiome: dysbioses and accumulation of resistances. *Front. Microbiol.* **6**, 1543
- Gronin, J. M., Tamura, K., Déjean, G., Abbott, D. W., and Brumer, H. (2017) Polysaccharide utilization loci: fueling microbial communities. *J. Bacteriol.* **199**, e00860-16
- Glowacki, R. W. P., and Martens, E. C. (2021) If you eat it or secrete it, they will grow: the expanding list of nutrients utilized by human gut bacteria. *J. Bacteriol.* **203**, e00481-20
- Dejean, G., Tamura, K., Cabrera, A., Jain, N., Pudlo, N. A., Pereira, G., et al. (2020) Synergy between cell surface glycosidases and glycan-binding proteins dictates the utilization of specific beta (1,3)-glucans by human gut bacteroides. *mBio* **11**, e00095-20
- Tamura, K., Foley, M. H., Gardill, B. R., Dejean, G., Schnizlein, M., Bahr, C. M. E., et al. (2019) Surface glycan-binding proteins are essential for cereal beta-glucan utilization by the human gut symbiont *Bacteroides ovatus*. *Cell. Mol. Life Sci.* **76**, 4319–4340
- Temple, M. J., Cuskin, F., Basle, A., Hickey, N., Speciale, G., Williams, S. J., et al. (2017) A *Bacteroidetes* locus dedicated to fungal 1,6-beta-glucan degradation: unique substrate conformation drives specificity of the key endo-1,6-beta-glucanase. *J. Biol. Chem.* **292**, 10639–10650
- Sheridan, O. P., Martin, J. C., Lawley, T. D., Browne, H. P., Harris, H. M. B., Bernalier-Donadille, A., et al. (2016) Polysaccharide utilization loci and nutritional specialization in a dominant group of butyrate-producing human colonic *Firmicutes*. *Microb. Genom.* **2**, e000043

27. La Rosa, S. L., Leth, M. L., Michalak, L., Hansen, M. E., Pudlo, N. A., Glowacki, R., et al. (2019) The human gut Firmicute *Roseburia intestinalis* is a primary degrader of dietary beta-mannans. *Nat. Commun.* **10**, 905
28. Liu, X., Mao, B., Gu, J., Wu, J., Cui, S., Wang, G., et al. (2021) *Blautia* a new functional genus with potential probiotic properties? *Gut Microbes* **13**, 1–21
29. Kim, S. G., Becattini, S., Moody, T. U., Shliaha, P. V., Littmann, E. R., Seok, R., et al. (2019) Microbiota-derived lantibiotic restores resistance against vancomycin-resistant *Enterococcus*. *Nature* **572**, 665–669
30. Caballero, S., Kim, S., Carter, R. A., Leiner, I. M., Susac, B., Miller, L., et al. (2017) Cooperating commensals restore colonization resistance to vancomycin-resistant *Enterococcus faecium*. *Cell Host Microbe* **21**, 592–602.e4
31. Singh, R. P., Rajarammohan, S., Thakur, R., and Hassan, M. (2020) Linear and branched β -glucans degrading enzymes from versatile *Bacteroides uniformis* JCM 13288^T and their roles in cooperation with gut bacteria. *Gut Microbes* **12**, 1–18
32. Chen, I. A., Chu, K., Palaniappan, K., Pillay, M., Ratner, A., Huang, J., et al. (2019) IMG/M v.5.0: an integrated data management and comparative analysis system for microbial genomes and microbiomes. *Nucleic Acids Res.* **47**, D666–D677
33. Tourlousse, D. M., Sakamoto, M., Miura, T., Narita, K., Ohashi, A., Uchino, Y., et al. (2020) Complete genome sequence of *Blautia producta* JCM 1471(T). *Microbiol. Resour. Announc.* **9**, e00141-20
34. Yang, M., Derbyshire, M. K., Yamashita, R. A., and Marchler-Bauer, A. (2020) NCBI's conserved domain database and tools for protein domain analysis. *Curr. Protoc. Bioinformatics* **69**, e90
35. Juncker, A. S., Willenbrock, H., Von Heijne, G., Brunak, S., Nielsen, H., and Krogh, A. (2003) Prediction of lipoprotein signal peptides in Gram-negative bacteria. *Protein Sci.* **12**, 1652–1662
36. Petersen, T. N., Brunak, S., von Heijne, G., and Nielsen, H. (2011) SignalP 4.0: discriminating signal peptides from transmembrane regions. *Nat. Methods* **8**, 785–786
37. Planas, A. (2000) Bacterial 1,3-1,4- β -glucanases: structure, function and protein engineering. *Biochim. Biophys. Acta* **1543**, 361–382
38. Viborg, A. H., Terrapon, N., Lombard, V., Michel, G., Czjzek, M., Henrissat, B., et al. (2019) A subfamily roadmap of the evolutionarily diverse glycoside hydrolase family 16 (GH16). *J. Biol. Chem.* **294**, 15973–15986
39. Jumper, J., Evans, R., Pritzel, A., Green, T., Figurnov, M., Ronneberger, O., et al. (2021) Highly accurate protein structure prediction with AlphaFold. *Nature* **596**, 583–589
40. Mirdita, M., Schütze, K., Moriwaki, Y., Heo, L., Ovchinnikov, S., and Steinegger, M. (2022) ColabFold: making protein folding accessible to all. *Nat. Methods* **19**, 679–682
41. Jain, N., Tamura, K., Dejean, G., Van Petegem, F., and Brumer, H. (2021) Orthogonal active-site labels for mixed-linkage endo-beta-glucanases. *ACS Chem. Biol.* **16**, 1968–1984
42. [preprint] Hallgren, J., Tsirigos, K. D., Pedersen, M. D., Almagro Armenteros, J. J., Marcatili, P., Nielsen, H., et al. (2022) DeepTMHMM predicts alpha and beta transmembrane proteins using deep neural networks. *bioRxiv*. <https://doi.org/10.1101/2022.04.08.487609>
43. Dvortsov, I. A., Lunina, N. A., Zverlov, V. V., and Velikodvorskaia, G. A. (2012) The properties of four C-terminal carbohydrate-binding modules (CBM4) of laminarinase Lic16A of *Clostridium thermocellum*. *Mol. Biol. (Mosk)* **46**, 915–921
44. Ejby, M., Fredslund, F., Andersen, J. M., Vujicic Zagar, A., Henriksen, J. R., Andersen, T. L., et al. (2016) An ATP binding cassette transporter mediates the uptake of α -(1,6)-linked dietary oligosaccharides in *Bifidobacterium* and correlates with competitive growth on these substrates. *J. Biol. Chem.* **291**, 20220–20231
45. Ejby, M., Fredslund, F., Vujicic-Zagar, A., Svensson, B., Slotboom, D. J., and Abou Hachem, M. (2013) Structural basis for arabinoxylo-oligosaccharide capture by the probiotic *Bifidobacterium animalis* subsp. *lactis* Bl-04. *Mol. Microbiol.* **90**, 1100–1112
46. Sakanaka, M., Hansen, M. E., Gotoh, A., Katoh, T., Yoshida, K., Odamaki, T., et al. (2019) Evolutionary adaptation in fucosylactose uptake systems supports *Bifidobacteria* infant symbiosis. *Sci. Adv.* **5**, eaaw7696
47. Parche, S., Amon, J., Jankovic, I., Rezzonico, E., Belet, M., Barutcu, H., et al. (2007) Sugar transport systems of *Bifidobacterium longum* NCC2705. *J. Mol. Microbiol. Biotechnol.* **12**, 9–19
48. Hirayama, Y., Sakanaka, M., Fukuma, H., Murayama, H., Kano, Y., Fukiya, S., et al. (2012) Development of a double-crossover markerless gene deletion system in *Bifidobacterium longum*: functional analysis of the alpha-galactosidase gene for raffinose assimilation. *Appl. Environ. Microbiol.* **78**, 4984–4994
49. Berntsson, R. P., Smits, S. H., Schmitt, L., Slotboom, D. J., and Poolman, B. (2010) A structural classification of substrate-binding proteins. *FEBS Lett.* **584**, 2606–2617
50. Cuneo, M. J., Beese, L. S., and Hellings, H. W. (2009) Structural analysis of semi-specific oligosaccharide recognition by a cellulose-binding protein of *Thermotoga maritima* reveals adaptations for functional diversification of the oligopeptide periplasmic binding protein fold. *J. Biol. Chem.* **284**, 33217–33223
51. Abe, K., Sunagawa, N., Terada, T., Takahashi, Y., Arakawa, T., Igarashi, K., et al. (2018) Structural and thermodynamic insights into β -1,2-glucooligosaccharide capture by a solute-binding protein in *Listeria innocua*. *J. Biol. Chem.* **293**, 8812–8828
52. Chandravanshi, M., Samanta, R., and Kanaujia, S. P. (2020) Conformational trapping of a beta-glucosides-binding protein unveils the selective two-step ligand-binding mechanism of ABC importers. *J. Mol. Biol.* **432**, 5711–5734
53. Wu, Y., Mao, G., Fan, H., Song, A., Zhang, Y. P., and Chen, H. (2017) Biochemical properties of GH94 celloidextrin phosphorylase THA_1941 from a thermophilic eubacterium *Thermosiphon africanus* TCF52B with cellobiose phosphorylase activity. *Sci. Rep.* **7**, 4849
54. Krishnareddy, M., Kim, Y. K., Kitaoka, M., Mori, Y., and Hayashi, K. (2002) Celloidextrin phosphorylase from *Clostridium thermocellum* YM4 strain expressed in *Escherichia coli*. *J. Appl. Glycosci.* **49**, 1–8
55. Sawano, T., Saburi, W., Hamura, K., Matsui, H., and Mori, H. (2013) Characterization of *Ruminococcus albus* celloidextrin phosphorylase and identification of a key phenylalanine residue for acceptor specificity and affinity to the phosphate group. *FEBS Lett.* **280**, 4463–4473
56. O'Neill, E. C., Pergolizzi, G., Stevenson, C. E. M., Lawson, D. M., Nepogodiev, S. A., and Field, R. A. (2017) Celloidextrin phosphorylase from *Ruminiclostridium thermocellum*: X-ray crystal structure and substrate specificity analysis. *Carbohydr. Res.* **451**, 118–132
57. Kuhadomlarp, S., Pergolizzi, G., Patron, N. J., Henrissat, B., and Field, R. A. (2019) Unraveling the subtleties of beta-(1->3)-glucan phosphorylase specificity in the GH94, GH149, and GH161 glycoside hydrolase families. *J. Biol. Chem.* **294**, 6483–6493
58. Holm, L., and Sander, C. (1995) Dali: a network tool for protein structure comparison. *Trends Biochem. Sci.* **20**, 478–480
59. Hidaka, M., Honda, Y., Kitaoka, M., Nirasawa, S., Hayashi, K., Wakagi, T., et al. (2004) Chitobiose phosphorylase from *Vibrio proteolyticus*, a member of glycosyl transferase family 36, has a clan GH-L-like (alpha/alpha)(6) barrel fold. *Structure* **12**, 937–947
60. Ruiz, L., Delgado, S., Ruas-Madiedo, P., Sanchez, B., and Margolles, A. (2017) *Bifidobacteria* and their molecular communication with the immune system. *Front. Microbiol.* **8**, 2345
61. O'Callaghan, A., and van Sinderen, D. (2016) *Bifidobacteria* and their role as members of the human gut microbiota. *Front. Microbiol.* **7**, 925
62. Canfora, E. E., Jocken, J. W., and Blaak, E. E. (2015) Short-chain fatty acids in control of body weight and insulin sensitivity. *Nat. Rev. Endocrinol.* **11**, 577–591
63. den Besten, G., van Eunen, K., Groen, A. K., Venema, K., Reijngoud, D. J., and Bakker, B. M. (2013) The role of short-chain fatty acids in the interplay between diet, gut microbiota, and host energy metabolism. *J. Lipid Res.* **54**, 2325–2340
64. Pluvinage, B., Grondin, J. M., Amundsen, C., Klassen, L., Moote, P. E., Xiao, Y., et al. (2018) Molecular basis of an agarose metabolic pathway acquired by a human intestinal symbiont. *Nat. Commun.* **9**, 1043
65. Boraston, A. B., Nurizzo, D., Notenboom, V., Ducros, V., Rose, D. R., Kilburn, D. G., et al. (2002) Differential oligosaccharide recognition by evolutionarily related beta-1,4 and beta-1,3 glucan-binding modules. *J. Mol. Biol.* **319**, 1143–1156

Utilizing mixed-linkage β -glucans by the *Blautia producta*

66. Theilmann, M. C., Fredslund, F., Svensson, B., Lo Leggio, L., and Abou Hachem, M. (2019) Substrate preference of an ABC importer corresponds to selective growth on beta-(1,6)-galactosides in *Bifidobacterium animalis* subsp. lactis. *J. Biol. Chem.* **294**, 11701–11711
67. Pichler, M. J., Yamada, C., Shuoker, B., Alvarez-Silva, C., Gotoh, A., Leth, M. L., et al. (2020) Butyrate producing colonic *Clostridiales* metabolise human milk oligosaccharides and cross feed on mucin via conserved pathways. *Nat. Commun.* **11**, 3285
68. Scott, K. P., Martin, J. C., Chassard, C., Clerget, M., Potrykus, J., Campbell, G., et al. (2011) Substrate-driven gene expression in *Roseburia inulinivorans*: importance of inducible enzymes in the utilization of inulin and starch. *Proc. Natl. Acad. Sci. U. S. A.* **108**, 4672–4679
69. Singh, R. P., Thakur, R., and Kumar, G. (2021) Human gut *Bacteroides uniformis* utilizes mixed linked β -glucans via an alternative strategy. *Bioact. Carbohydr. Dietary Fibre* **26**, 100282
70. Biddle, A., Stewart, L., Blanchard, J., and Leschine, S. (2013) Untangling the genetic basis of fibrolytic specialization by *Lachnospiraceae* and *Ruminococcaceae* in diverse gut communities. *Diversity* **5**, 627–640
71. Zhang, Y. J., Li, S., Gan, R. Y., Zhou, T., Xu, D. P., and Li, H. B. (2015) Impacts of gut bacteria on human health and diseases. *Int. J. Mol. Sci.* **16**, 7493–7519
72. Moroti, C., Souza Magri, L. F., de Rezende Costa, M., Cavallini, D. C., and Sivieri, K. (2012) Effect of the consumption of a new symbiotic shake on glycemia and cholesterol levels in elderly people with type 2 diabetes mellitus. *Lipids Health Dis.* **11**, 29
73. Chen, J., Wang, R., Li, X. F., and Wang, R. L. (2012) *Bifidobacterium adolescentis* supplementation ameliorates visceral fat accumulation and insulin sensitivity in an experimental model of the metabolic syndrome. *Br. J. Nutr.* **107**, 1429–1434
74. Watanabe, Y., Saito, Y., Hara, T., Tsukuda, N., Aiyama-Suzuki, Y., Tanigawa-Yahagi, K., et al. (2021) Xylan utilisation promotes adaptation of *Bifidobacterium pseudocatenulatum* to the human gastrointestinal tract. *ISME Commun.* **1**, 62
75. Zhao, L., Zhang, F., Ding, X., Wu, G., Lam, Y. Y., Wang, X., et al. (2018) Gut bacteria selectively promoted by dietary fibers alleviate type 2 diabetes. *Science* **359**, 1151–1156
76. Nomura, S., Sukowati, E. W., Shigeno, Y., Takahashi, M., Kato, A., Benno, Y., et al. (2023) *Blautia coccoides* JCM1395^T achieved intratumoral growth with minimal inflammation: evidence for live bacterial therapeutic potential by an optimized sample preparation and colony PCR method. *Pharmaceutics* **15**, 989
77. Parada Venegas, D., De la Fuente, M. K., Landskron, G., Gonzalez, M. J., Quera, R., Dijkstra, G., et al. (2019) Short chain fatty acids (SCFAs) mediated gut epithelial and immune regulation and its relevance for inflammatory bowel diseases. *Front. Immunol.* **10**, 277
78. Seo, B., Jeon, K., Moon, S., Lee, K., Kim, W. K., Jeong, H., et al. (2020) *Roseburia* spp. abundance associates with alcohol consumption in humans and its administration ameliorates alcoholic fatty liver in mice. *Cell Host Microbe* **27**, 25–40
79. Chia, L. W., Hornung, B. V. H., Aalvink, S., Schaap, P. J., de Vos, W. M., Knol, J., et al. (2018) Deciphering the trophic interaction between *Akkermansia muciniphila* and the butyrogenic gut commensal *Anaerostipes caccae* using a metatranscriptomic approach. *Antonie van Leeuwenhoek* **111**, 859–873
80. Kamiya, T., Tang, C., Kadoki, M., Oshima, K., Hattori, M., Saijo, S., et al. (2018) β -Glucans in food modify colonic microflora by inducing antimicrobial protein, calprotectin, in a Dectin-1-induced-IL-17F-dependent manner. *Mucosal Immunol.* **11**, 763–773
81. Zheng, D., Liwinski, T., and Elinav, E. (2020) Interaction between microbiota and immunity in health and disease. *Cell Res.* **30**, 492–506
82. Singh, R. P., Prakash, S., Bhatia, R., Negi, M., Singh, J., Bishnoi, M., et al. (2020) Generation of structurally diverse pectin oligosaccharides having prebiotic attributes. *Food Hydrocolloids* **108**, 105988
83. Singh, R. P., Bhaiyya, R., Thakur, R., Niharika, J., Singh, C., Latousakis, D., et al. (2022) Biochemical basis of xylooligosaccharide utilisation by gut bacteria. *Int. J. Mol. Sci.* **26**, 2992
84. Macdonald, S. S., Armstrong, Z., Morgan-Lang, C., Osowiecka, M., Robinson, K., Hallam, S. J., et al. (2019) Development and application of a high-throughput functional metagenomic screen for glycoside phosphorylases. *Cell Chem. Biol.* **26**, 1001–1012.e5
85. McKee, L. S. (2017) Measuring enzyme kinetics of glycoside hydrolases using the 3,5-dinitrosalicylic acid assay. *Methods Mol. Biol.* **1588**, 27–36
86. Altschul, S. F., Gish, W., Miller, W., Myers, E. W., and Lipman, D. J. (1990) Basic local alignment search tool. *J. Mol. Biol.* **215**, 403–410
87. Kumar, S., Stecher, G., Li, M., Knyaz, C., and Tamura, K. (2018) MEGA X: Molecular evolutionary genetics analysis across computing platforms. *Mol. Biol. Evol.* **35**, 1547–1549
88. Olafsdottir, E. S., and Ingolfsdottir, K. (2001) Polysaccharides from lichens: structural characteristics and biological activity. *Planta Med.* **67**, 199–208
89. Morales, D., Rutkevski, R., Villalva, M., Abreu, H., Soler-Rivas, C., Santoyo, S., et al. (2020) Isolation and comparison of alpha- and beta-D-glucans from shiitake mushrooms (*Lentinula edodes*) with different biological activities. *Carbohydr. Polym.* **229**, 115521
90. Hamura, K., Saburi, W., Abe, S., Morimoto, N., Taguchi, H., Mori, H., et al. (2012) Enzymatic characteristics of cellobiose phosphorylase from *Ruminococcus albus* NE1 and kinetic mechanism of unusual substrate inhibition in reverse phosphorolysis. *Biosci. Biotechnol. Biochem.* **76**, 812–818
91. Honda, Y., Kitaoka, M., and Hayashi, K. (2004) Reaction mechanism of chitobiose phosphorylase from *Vibrio proteolyticus*: identification of family 36 glycosyltransferase in *Vibrio*. *Biochem. J.* **377**, 225–232
92. Kitaoka, M., Sasaki, T., and Taniguchi, H. (1992) Phosphorolytic reaction of *cellvibrio gilvus* cellobiose phosphorylase. *Biosci. Biotechnol. Biochem.* **56**, 652–655
93. Nidetzky, B., Eis, C., and Albert, M. (2000) Role of non-covalent enzyme-substrate interactions in the reaction catalysed by cellobiose phosphorylase from *Cellulomonas uda*. *Biochem. J.* **351**, 649–659